Title

Development of Dimethylisoxazole-Attached Imidazo[1,2-a]pyridines as Potent and Selective CBP/P300 Inhibitors

Journal

Journal of Medicinal Chemistry, 64(9)

ISSN

0022-2623

Authors

Muthengi, Alex
Wimalasena, Virangika K
Yosief, Hailemichael O
et al.

Publication Date

2021-05-13

DOI

10.1021/acs.jmedchem.0c02232

Peer reviewed

HHS Public Access

Author manuscript

J Med Chem. Author manuscript; available in PMC 2022 February 18.

Published in final edited form as:

J Med Chem. 2021 May 13; 64(9): 5787–5801. doi:10.1021/acs.jmedchem.0c02232.

Development of Dimethylisoxazole-attached Imidazo[1,2-*a*]pyridines as Potent and Selective CBP/P300 Inhibitors

Alex Muthengi[a,h], **Virangika K. Wimalasena**[b,h], **Hailemichael O. Yosief**[a,h], **Melissa J. Bikowitz**[c,d,h], **Logan H. Sigua**[b], **Tingjian Wang**[b], **Deyao Li**[b], **Zied Gaieb**[e], **Gagan Dhawan**[f], **Shuai Liu**[a], **Jon Erickson**[a], **Rommie E. Amaro**[e], **Ernst Schönbrunn**[c,d,*], **Jun Qi**[b,g,*], **Wei Zhang**[a,*]

[a]Center for Green Chemistry and Department of Chemistry, University of Massachusetts Boston, 100 Morrissey Boulevard, Boston, MA 02125, USA

[b]Department of Cancer Biology, Dana-Farber Cancer Institute, 450 Brookline Avenue, Boston, MA 02215, USA

[c]Drug Discovery Department, Moffit Cancer Center, Tampa, FL 33612, USA

[d]Department of Molecular Medicine, USF Morsani College of Medicine, University of South Florida, Tampa, FL 33612, USA

[e]Department of Chemistry & Biochemistry, University of California, San Diego, 9500 Gilman Dr, LA Jolla, CA 92093, USA

[f]Department of Biomedical Science, Acharya Narendra Dev College, University of Delhi, New Delhi-110019, India

[g]Department of Medicine, Harvard Medical School, 220 Longwood Avenue, Boston, MA 02115, USA

[h]These authors contributed equally to this work

Abstract

[*]**Corresponding Authors** Ernst.Schonbrunn@moffitt.org. Tel.: +1 (813) 745-4703. Fax: +1 (813) 745-6748, jun_qi@dfci.harvard.edu. Tel.: +1 (617) 632-6629. Fax: +1(617) 582-7370, wei2.zhang@umb.edu. Tel.: +1 (617) 287-6147. Fax: +1 (617) 287-6030.

Author Contributions

All authors have given approval to the final version of the manuscript.

ASSOCIATED CONTENT

Supporting Information

BromoSCAN®, differential scanning fluorometry (DSF) and cellular activity data of compounds **7**, **16**, and **23;** Crystallographic data collection and refinement statistics of compound **23;** ^{1}H-NMR & ^{13}C-NMR of representative compounds; HPLC traces of compounds **7**, **16**, and **23** (PDF)

Molecular-formula strings (CSV)

Homology (Docking) Models of BRD4_5BT4_Cpd7 (UMB276), BRD4_5BT4_Cpd-16 (UMB295), BRD4_5BT4_Cpd-23 (UMB298), CBP_4NR7_Cpd-3 (UMB274), CBP_4NR7_Cpd-4 (UMB278), CBP_4NR7_Cpd-7 (UMB276), CBP_4NR7_Cpd-16 (UMB295), CBP_4NR7_Cpd-23 (UMB298) (PDB)

Co-crystallographic data of compound **23** (UMB298) (PDB)

Accession Codes

PDB accession code for co-crystal structure of CBP bromodomain liganded with compound **23** (UMB298) is 7KPY. Authors will release the atomic coordinates upon article publication.

Dr. Jun Qi is a scientific co-founder and shareholder of Epiphanes.

The use of epigenetic bromodomain inhibitors as anti-cancer therapeutics has transitioned from targeting bromodomain extra terminal (BET) proteins into targeting non-BET bromodomains. The two most relevant non-BET bromodomain oncology targets are cyclic AMP response element-binding protein (CBP) and E1A binding protein P300 (EP300). To explore the growing CBP/EP300 interest, we developed a highly efficient two-step synthetic route for dimethylisoxazole-attached imidazo[1,2-*a*]pyridine scaffold-containing inhibitors. Our efficient two-step reactions enabled high-throughput synthesis of compounds designed by molecular modeling which together with structure activity relationship (SAR) studies facilitated overarching understanding of selective targeting of CBP/EP300 over non-BET bromodomains. This led to identification of a new potent and selective CBP/EP300 bromodomain inhibitor, UMB298 (compound **23**, CBP IC_{50} 72 nM and BRD4 IC_{50} 5193 nM). The SAR we established is in good agreement with literature reported CBP inhibitors, such as CBP30, and demonstrates the advantage of utilizing our two-step approach for inhibitor development of other bromodomains.

Graphical Abstract

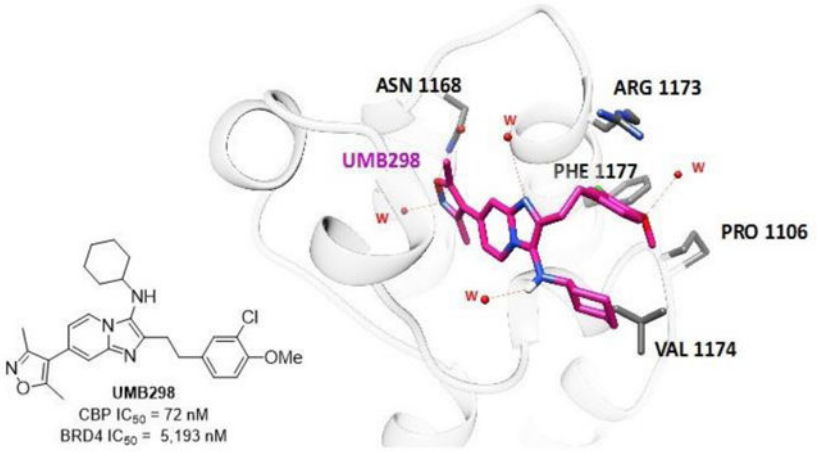

INTRODUCTION

Bromodomains (BRDs) are epigenetic reader domains that selectively recognizing acetyl-lysine residues found in histone and non-histone proteins, and function in transcriptional regulation.[1–3] Failure to regulate these protein reader modules can result in a broad range of diseases such as cancer, inflammatory and cardiovascular diseases. As a result, they are pursued as attractive targets for developing therapeutic agents for the treatment of different disease conditions.[4,5] Although much progress has been made in the development BET bromodomain small molecule inhibitors, some of which are are undergoing human clinical trials for various diseases,[1,2] selective and potent non-BET bromodomains inhibitors and use in biological studies is still limited. Out of the 57 non-BET bromodomains, the CBP bromodomain which was one considered to have “medium druggability”, has generated recent interest in oncology applications and 3 new double digit nanomolar inhibitors have been developed.[6–8] Additionally, CBP has a paralog that conducts similar activity called E1A binding protein (EP300 or P300), both of which are multi-domain proteins containing

BRD and other domains, such as lysine acetyl transferase (KAT) which acetylates and recruits histone and non-histone proteins.

Overview of the role of CBP/EP300 in disease.

The BRD of CBP/EP300 selectively recognizes acetylated lysine residues, in contrast to the KAT domain, which acetylates lysine residues on both histone tails and signature tumor transcription factors, such as p53 and c-*MYC*.[9–12] There are 8 acetylation sites on p53, of which K382 is necessary for co-activator (CBP and TRRAP) recruitment which importantly results in a p53 stabilizing conformation change, and therefore active p53 and activation of pro-apoptotic genes.[13,14] The CBP/P300 bromodomains have been linked to disorders like acute myeloid leukemia (AML), inflammatory and neurodegenerative diseases. [15, 16] Recently, Olzscha and co-workers also demonstrated that CBP/P300 bromodomains are required for protein aggregation which disturbs proteostasis by impairing the ubiquitin proteasome system (UPS) and protein translation, leading to decreased cell viability.[17] Overall, CBP/EP300 are considered the most promising non-BET bromodomain targets for cancer and other pathological conditions.[8] Therefore, this study was aimed at developing a novel strategy to discover potent and selective CBP inhibitors for use as chemical probes to provide further insight into CBP/EP300-disease pathogenesis.

Inhibitors targeting the bromodomain of CBP/EP300.

According to the Structural Genomics Consortium (SGC) requirement, a chemical probe should possess inhibitory activity at less than 100 nM concentration (IC_{50} <100 nM), with selectivity greater than 30 fold toward other proteins (>30 fold) and cellular activity at ~ 1 μM concentration.[18,19] To better understand and investigate the biological function of CBP bromodomains, a number of CBP inhibitors have been reported with submicromolar to nanomolar inhibitory activity against the bromodomain of CBP or P300, including CBP30,[10] R-2,[20] PF-CBP1,[9,21] TPO146,[22] CPI-637[23], GNE-272[24] and GNE-781[25] (Figure 1). Most of these compounds are prepared through multi-step synthesis with low overall yields, which hampers further optimization of the compounds to improve their biological activity.[10] We have recently reported a two-step synthesis of dimethylisoxazole-attached imidazo[1,2-*a*]pyridine BET inhibitors.[26] Overall, we envisioned we could employ the optimized two-step synthetic route toward developing new CBP/EP300 inhibitors in conjunction with structure activity relationship (SAR) studies to generate lead compounds. Additionally, the methods can be further extended to the development of inhibitors targeting other bromodomains.

RESULTS AND DISCUSSION

Analysis of the chemical structures of reported CBP inhibitors revealed that potent inhibitors contain two important components. The first is an acetyl-lysine mimic motif (blue unit in the structures showed in Figure 1) such as 3,5-dimethylisoxazole and the second is an appendix portion outside the binding pocket, such as 3-chloro-4-methoxyphenethyl and ethylmorpholinyl motifs which can engage in additional interactions with the protein outside the binding pocket. This analysis inspired us to use our modified multicomponent

reaction (MCR) to assemble a substituted imidazo[1,2-*a*]pyridine scaffold followed by the introduction of a binding motif through the Suzuki coupling (Scheme 1).[26]

By utilizing our highly efficient synthesis involving three-component Groebke−Blackburn−Bienayme (GBB)[27–29] reactions followed by the Suzuki coupling reaction,[26, 30] we generated a set of molecules with different binding motifs linked to imidazo[1,2-*a*]pyridine scaffold in two steps. These compounds were assessed for their binding activity against CBP bromodomain utilizing an AlphaScreen assay using biotinylated peptide and recombinant CBP bromodomain as assay partners (Table 1) and against BRD4 in our previously developed BRD4 AlphaScreen assay.[31] Overall, AlphaScreen showed the compounds exhibited selective micromolar inhibitory activity against CBP bromodomain, over BRD4. Significant improved potency and selectivity was seen when the known strong acetylated-lysine mimetic (3,5-dimethylisoxazole) substituent group[32, 33] was introduced at R^2 position (Table 1). Previous studies showed that 3,5-dimethylisoxazole acts as an acetyl lysine mimic, where the isoxazole oxygen forms a hydrogen bonding interaction with the Asn1168 amide moiety while isoxazole nitrogen points toward one of the water molecules that bridges with the Tyr1125.[10, 26] Interestingly, compound **4** exhibited modest inhibitory activity against CBP and BRD4 with an IC_{50} of 1.17 μM and 2.96 μM respectively. These promising data indicated that our strategy could facilitate SAR studies to fine tune the potency and selectivity in a high throughput manner. Encouraged by these results, we decided to fully explore the CBP inhibitor design and development using imidazo[1,2-*a*]pyridine scaffold as core (Table 1).

While the peptide based AlphaScreen assay can assess compound activity, the performance of this assay is not robust due to the limited stability of the peptide used. We therefore developed a novel small molecule-based AlphaScreen assay for CBP and EP300 bromodomain using biotinylated probe **C** (Scheme 2) with recombinant proteins (Figure 2). Since the bromodomains of EP300 and CBP have greater than 95% homology, we utilized the CBP bromodomain to represent both CBP and EP300 bromodomains. This probe compound was derivatized from compound **2** shown in Table 1 guided by the co-crystal structure of CBP30 with CBP (PDB ID: 4NR7) reported in the literature. In this assay, biotinylated compound **C** was utilized as a novel probe to evaluate the competitive displacement by our series of CBP bromodomain inhibitors. Purified His-tagged CBP or EP300 bromodomain bound to Nickel beads and biotinylated compound **C** bound to Streptavidin beads were brought into close proximity to one another upon probe binding to protein. Upon excitation, the beads created an emission due to their proximity, which was disrupted by competitive binding by our bromodomain inhibitors, displacing the probe, allowing for a dose response binding curve to be extrapolated. To optimize the assay condition, we systematically titrated both ligand (**C**) and protein (His-CBP) against each other at varying concentrations in the presence of 20 ng/mL Streptavidin donor beads & 20 ng/mL Nickel Acceptor beads. As these are standard Alpha bead concentrations, this 2D titration is performed to yield an optimal Alphascreen signal. Because we are forming a ternary complex in this Alphascreen reaction, there is an optimal “hook point” concentration that correlates with optimal signal.[31] We titrated both the compounds ranging from 10 uM to 5 nM and found that Compound C was able to generate this characteristic hook point

at 10 nM ligand concentration, and 50 nM His-tagged CBP protein concentration. We have further confirmed the signal intensity of the small molecule probe based assay is similar as the peptide based assay. The small molecule probed based assay perform more consistent compared to peptide based assay and used for the IC50 assessment for establishing SAR.

To have a better understanding of the observed potency and selectivity, we utilized molecular modeling to explore the binding modes of our imidazo[1,2-*a*]pyridine inhibitor compound **4** (UMB278) with CBP using co-crystal structure of CBP30 with CBP bromodomain (Figure 3). The isoxazole of compound **4** showed critical hydrogen bonding with N1168, mimicking the acetylated lysine interaction observed between CBP and its substrate. We observed extra hydrogen bonds around imidazo[1,2-*a*]pyridine with surrounding crystallographic water molecules that might also contribute favorably to binding activity. Thus, we decided to maintain the 3,5-dimethylisoxazole as a warhead and imidazo[1,2-*a*]pyridine as a scaffold because they are responsible for the improved inhibitory activity of our inhibitors. We noticed that the solvent accessible methoxy phenyl group might contribute to the low affinity of the molecules since the planarity of the bond between the benzimidazole and the benzene groups might prohibit the molecules from forming cation-π interactions with R1173. Thus, we explored the effect of modifying the two appendix groups R^1 and R^3 (Table 2).

Based on our hypothesis, we introduced a rotatable bond between methoxy-phenyl and imidazo[1,2-*a*]pyridine to extend the appending group and increase the binding interactions with R1173 on the CBP bromodomain outside the binding pocket (Table 2). We synthesized compounds by introducing a two-carbon linker between the core structure and the 4-methoxyphenyl group. The extension of the phenyl group in compounds **7** and **8** led to improved potency and selectivity compared to compound **4**, suggesting that the flexibility we introduced allows the R^3 position to contribute additional interactions with the target site. Usually, the two-carbon linker's flexibility allows the R3 position to contribute additional interactions with the active site. Compound **6** is exception that may be due to a different binding mode/ preferred orientation of compound **6** in the drug-receptor complex. The lifetime of the Drug-Receptor complex is a dynamic process. This can also be explained by the duration of time that the drug-receptor complex persists i.e. residence time - maybe it readily dissociates from their target receptor. We continued to explore whether this improved potency and selectivity could apply to other acetyl lysine mimics. By taking advantage of our two-step synthesis, other warheads like 3-methyl-3,4-dihydroquinazolin-2(1*H*)-one (compound **9**), 3-methyl-2*H*-indazole (compound **10**), and 3-methyl-3a,7a-dihydrobenzo[*d*]isoxazole (compound **11**) were introduced to the core via Suzuki coupling. These warheads, however, showed a greater than 10-fold loss in inhibitory activity against CBP (Table 2). This is due to the difference in the moieties' size, the induced fit is different. The distance between the key/critical hydrogen-bond acceptors of the acetylated lysine mimic and the imidazopyridine core increases, leading to a decrease in hydrogen bonding affinity. Compound **10** and **11** displayed greater than 15-fold increase in inhibitory activity against BRD4 (Table 2). This result reinforced our interest to use 3,5-dimethylisoxazole as the warhead for CBP bromodomain inhibitor development. We next explored the R^1 position by introducing different polar and hydrophobic groups. Use of cyclohexyl group at R^1 while maintaining a methoxy group at R^3 led to a potent and

selective inhibitor, compound **16**, with CBP and BRD4 inhibitory potencies of 0.159 μM and 6.59 μM, respectively (Table 2). When *t*-butyl (compound **13** and **18**), and adamantyl (compound **14**) groups were introduced at the R^1 position, CBP inhibitory activity decreased by >5-fold, while use of 4-ethylmorpholinyl (compound **15**) and isopropyl (compound **17**) led to roughly a 2 and 3-fold decrease in potency respectively (Table 2). Unfortunately, use of benzyl groups for R^1, compound **21** and **22**, led to 10-fold decrease in CBP inhibitory potency (Table 2). At the same time, we observed that compound **16** exhibited a 5-fold increase in CBP inhibitory potency compared to compound **7** which lacks an electron donating group, *p*-methoxy, on the aryl ring.

Subsequently, we assessed the impact of different alkyl groups at the R^3 position (Table 2). The ethoxy group (compound **19**) showed a subtle decrease in potency against the CBP bromodomain compared to compound **16**, while the introduction of the propyloxyl group (compound **20**) caused a ~4-fold decrease in potency (Table 2). Therefore, the *p*-methoxy group on the aryl ring was retained as it proved to be important for the increased CBP inhibitory activity without compromising selectivity (41-fold) against BRD4.

Molecular docking confirmed that the presence of an electron donating group, *p*-methoxy, on the aryl ring further reinforces the cation-π interactions of the CBP inhibitor with the Arg1173 of the CBP bromodomain (Figure 4). Additionally, the hydrophobic methyl in the methoxy group of compound **16** stabilizes solvent accessible hydrophobic residues on the protein side (PRO1106, Val1174, and Phe1177). Compound **16** exhibited improved binding affinity to CBP compared to compounds **3**, **4** and **7** (Figures 3 & 4).

Our highly efficient two-step synthesis entitled us to quickly explore the SAR around the core of compound **16** by introducing substituent group(s) on the phenyl ring of *p*-methoxyphenyl group as well as by changing the distance between phenyl ring and imidazo[1,2-*a*]pyridine (Table 3). First, we hypothesized that the introduction of a halogen group could further improve the potency against CBP by promoting electrostatic interactions with the target, and also increase lipophilicity of the compound; consistent with previous reports.[10] Indeed, introduction of a *m*-chloro group at the aryl ring resulted in a more potent and selective CBP inhibitor, compound **23**, CBP IC_{50} 72 nM and BRD4 IC_{50} 5193 nM, which was 2-fold more potent than compound **16**. Additionally, compound **23** displayed 72-fold selectivity for CBP over BRD4 as a selective CBP inhibitor (Table 3). Notably, we discovered that the distance between the phenyl ring and the imidazo[1,2-*a*]pyridine is also important, as evidenced by the large impact on potency seen with different linker lengths. Reducing the length of the linker to methylene (compound **24** compared to compound **16**), or increasing the length (compound **25** and **30** compared to compound **23**) led to a loss of CBP inhibitory activity, while maintaining BRD4 activity (less than 2 fold). Therefore, we identified the optimal linker for this scaffold and the importance of introducing the chloro-methoxy-phenyl group. In this compound series, the cyclohexyl was the optimal group for R^1, while other groups led to loss of activity (compounds **26**-**28**, and **34** (Table 3)). Since an electron donating moiety was well tolerated on the aryl group connecting the liner (compound 23); we decided to introduce two hydrogen bond acceptors, m and p-methoxy groups. Surprisingly, CBP inhibitory potency was lost by ~10 fold, with insignificant change in BRD4 activity (compound **32**) (Table 3), indicating that *m*-chloro group was important for

improved activity of compound **23**. Similarly, use of isopropyl for R^1, compound **33**, led to 49-fold and 4-fold loss in CBP and BRD4 inhibitory activity respectively (Table 3).

The docking model provided the explanation to this improvement. Introduction of the halogen group (*m*-Cl) in compound **23** further stabilizes the solvent accessible environment around the aryl group and R1173 (Figure 5A) thus improving binding affinity. Analysis of the binding poses of compound **23** or CBP30 with CBP showed no clear difference between the benzimidazole of CBP30 and the imidazopyridine of compound **23** (Figure 6A-B). The low affinity for BRD4 of the three compounds is due to the methyl (in the OMe group) and the cyclohexyl groups being completely solvent exposed in BRD4 (Figure 5B). R1173 in CBP anchors the ethylene linker in compounds **7**, **16**, and **23** by forming cation-π interactions with the aryl group. However, R1173 is replaced by D145 in BRD4. This amino acid difference abolishes the receptor's ability to form cation-π interactions with molecules in the binding pocket of BRD4 and rationalizes the selectivity that emerges for compounds **7**, **16**, and **23**. Overall, the docking analysis of compound **4**, **7**, **16**, and **23** with CBP and BRD4 bromodomain was consistent with the binding affinities obtained in our biochemical assays.

Excitingly, we have obtained the co-crystal structure of compound **23** (UMB298) with bromodomain of CBP (Figure 6C-D). As expected from our docking model, the crystal structure confirmed that the 1,3-dimethyl isoxazole ring acted as a acetyl lysine mimetic to interact with the conserved Asn1168. The fused imidazo[1,2-*a*]pyridine core showed the same orientation as CBP30 (Figure 6A), and extended the chloro, methoxyl phenyl group into the pocket formed by Arg 1173 and Phe 1177 as predicted by docking. This extension further explains the CBP selectivity we observed with our lead molecule **23** and confirms the accuracy of our docking model.

Selectivity assessment and cellular activity.

To further confirm the selectivity observed in our biochemical assay, we utilized differential scanning fluorometry (DSF) to measure the binding of compounds with BRD4 BD1 (the first bromodomain of BRD4), CBP bromodomain, and EP300 (P300) bromodomain (Figure S1, Figure 7A). Compound **7** showed very modest activity toward BRD4, but was more active against CBP and EP300. Compounds **16** and **23** showed greater selectivity than the known inhibitor, CBP30, with slightly reduced potency. Further profiling using BROMOSCAN® against 34 bromodomains at 1 μM compound concentration showed promising binding and selectivity values for the three compounds, with compound **23** having a better binding and selectivity compared to compound **7** and **16** (Figure 7B and Table S1). The binding affinity (Kd) of compound **16** and **23** were further confirmed by BromoELECT^{SM} with CBP, EP300 and BRD4 (BD1). We observed similar binding trends and comparable selectivity to our AlphaScreen data.

We next evaluated the cellular activity of our lead molecule **23** in the AML cell line MOLM13 and several multiple myeloma lines in comparison with CBP30. Compound **23** inhibited MOLM13 and MM cell growth with IC50 values similar to CBP30 (Figure 8A and Figure S2). These compounds can inhibit the leukemia cell growth at high concentration

as described in literature that the CBP/EP300 bromodomain inhibitor alone has limited effect on blocking CBP/EP300 functions.[18, 35] We further investigated on-target inhibition of our compounds by checking the impact of bromodomain inhibition on H3K27ac and Myc expression levels. Treatment with compound **23** reduced the H3K27ac level similar to CBP30, and caused MYC depletion as a signature of CBP inhibition in AML (Figure 8B). The MYC level reduction was further confirmed by RT-PCR experiments (Figure 8C). To confirm compound **23** exerted MYC deletion through on-target CBP/EP300 inhibition, we assessed the effect of selective CBP inhibitor (CBP30 and compound **23**) for their effect on IRF4/MYC function in multiple myeloma cell line (MM.1S)[36] using compound **10** and **11**, selective toward BRD4 as negative control. We observed the IRF4/MYC axis was perturbed by CBP30 and compound **23** at similar level but not with BRD4 inhibitor as we expected (Figure 8D).[36] The compound **23** showed similar but slightly weaker cellular activity compared to CBP30 that matches the binding activities we observed in biochemical assays. Thus, the core we built with our GBB reaction can produce the EP300/CBP inhibitors with good cellular activity.

CONCLUSIONS

Developing potent inhibitors that can disrupt protein-protein interactions remains a challenging but attractive task for drug development.[37] In this work, we have developed an effective synthetic method to assemble the core of a panel of potent bromodomain inhibitors. Our two-step synthesis involved the Groebke−Blackburn−Bienayme (GBB) reaction[27–29] to build the core and decorate the core with various functional groups and different appendix groups in a relatively high throughput manner. The Suzuki coupling installed the acetyl lysine mimetic with a high overall yield (>90%). The approach generated a broad spectrum of compounds with different potency and selectivity against CBP over BRD4. In parallel, we established a computational model that explains the observed potency and selectivity. The model provided valuable information which aided the rational design of novel potent and selective inhibitors. More importantly, this model and the related explanation have been further confirmed by the co-crystal structure of our lead molecule compound **23** with CBP bromodomain. The lead compound **23** built upon the imidazo[1,2-*a*]pyridine scaffold with optimization on other parts (R^{1-3}) of the molecule showed comparable potency and selectivity with other reported CBP inhibitors in biochemical and cellular assays. Compared to the synthetic approaches previously employed for the synthesis of reported CBP inhibitors, our method is simple and resource efficient, allowing quick and comprehensive SAR studies. Compound **23** qualifies that can be used to assist in the interrogation of the biological roles of this protein in diseases. More importantly, we envision our novel and effective approach can be utilized for bromodomain inhibitor development targeting other bromodomains outside the BET and CBP/EP300 family.

EXPERIMENTAL SECTION

Chemistry.

The synthesis of imidazo[1,2-*a*]pyridine scaffold based CBP inhibitors was done in two steps; three-component reaction[27–29] followed by the Suzuki coupling.[30, 38] Synthesis

of compound **23** involved multicomponent reaction by combining 4-bromopyridin-2-amine, 3-(3-chloro-4-methoxyphenyl)propanal and cyclohexylisocyanide, under microwave irradiation for 40 min. This was followed by the Suzuki coupling of the intermediate with 3,5-dimethylisoxazole-4-boronic acid pinacol ester. Both steps had yields and produced the final product with an overall good yield. It's a green synthesis with high overall yield, atom- and step economy. Previously, the Brennan group reported CBP30, a potent and selective CBP inhibitor, (CBP, IC_{50} = 79 nM) with a selectivity window of 40 fold against BRD4.[9] It contains a benzimidazole scaffold.[9] The synthesis of CBP30 involved five steps through a linear or multistep synthesis; leading to low overall yield of about 4%.[9] In this study an imidazo[1,2-*a*]pyridine scaffold was used, with substituent groups around the imidazo[1,2-*a*]pyridine scaffold varied by use of different aldehydes, isocyanides and also warheads as acetyl lysine mimic, 3,5-dimethylisoxazole, 3-methyl-2H-indazole, 3-methyl-3a,7a-dihydrobenzo[*d*]isoxazole and 3-methyl-3,4-dihydroquinazolin-2(*1H*)-one to get a panel of compounds (Scheme 1). The synthesized compounds were screened for their inhibitory activity against CBP and BRD4 using AlphaScreen assay to obtain IC_{50} values.

General Synthetic Information.

Chemicals and solvents were purchased from commercial suppliers and used as received. All the compounds used for biological assay were >95% pure as determined by NMR and LC-MS. ^{1}H NMR (400 MHz) and ^{13}C NMR spectra (101 MHz) were recorded on Agilent NMR spectrometers. The chemical shifts were reported in parts per million (ppm), and the residual solvent peak was used as an internal reference: proton (chloroform δ 7.26) and carbon (chloroform δ 77.0). Multiplicities were indicated as follows: s (singlet), d (doublet), t (triplet), q (quartet), m (multiplet), dd (doublet of doublet), br s (broad singlet). Coupling constants were reported in hertz (Hz). LC–MS was performed on an Agilent 2100 LC with a 6130 quadruple MS spectrometer, and a C18 column (5.0 μm, 6.0 × 50 mm) was used for separation. The mobile phases were MeOH and H_2O; both containing 0.01% trifluoroacetic acid. A linear gradient of 50:50 (v/v) MeOH/H_2O to 100% MeOH was used over 7.0 min at a flow rate of 0.7 mL/min. The chromatograms were detected at UV wavelengths 210, 254, and 365 nm. Low resolution mass spectra were recorded in APCI (atmospheric pressure chemical ionization). The microwave reactions were performed on a Biotage Initiator 8 system equipped with an Infrared (IR) sensor (external surface sensor) to monitor the reaction temperature. Flash chromatography separation was performed on YAMAZEN AI-580 system with Agela silica gel (12 or 20 g, 230−400 μm mesh) cartridges. Some of the final products were purified using Agela HP-100 pre-LC system with a Venusil PrepG C18 column (10 μm, 120 Å, 21.2 mm × 250 mm). HRMS was analyzed by RP-LC-MS: 1 μL of each sample was combined and 500 mL of optima grade MeCN (0.1 % formic acid) and 500 mL of optima grade H_2O (0.1 % formic acid) were added to the mixture. This mixture was then diluted by another factor of 10 with a 75/25 mixture of the optima grade MeCN and H_2O. 1 mL (10 fmol of each on column) of this mixture was analyzed by RP-LC-MS. The mass analyzer was orbitrap.

Synthesis of Biotinylated-CBP/P300 Bromodomain Binder C.

5-(4-(4-(3-(cyclohexylamino)-6-(3,5-dimethylisoxazol-4-yl)imidazo[1,2-a]pyridin-2-yl)phenyl)piperazin-1-yl)-5-oxopentanoic acid (compound

B).—To the solution of **A** (20.0 mg, 0.0394 mmol) and DIPEA (13.2 uL, 0.0788 mmol) in DCM (2 mL) was added glutaric anhydride (6.74 mg, 0.0591 mmol) at room temperature. The mixture was stirred at room temperature for 4 hours and then purified *via* ISCO (MeOH/DCM = 0 ~ 15%) to afford **B** as colorless oil (18.0 mg, 78% yield). MS: m/z $(M+1)^+$: 585.27.

5-(4-(4-(3-(cyclohexylamino)-6-(3,5-dimethylisoxazol-4-yl)imidazo[1,2-a]pyridin-2-yl)phenyl)piperazin-1-yl)-5-oxo-N-(15-oxo-19-((4S)-2-oxohexahydro-1H-thieno[3,4-d]imidazol-4-yl)-4,7,10-trioxa-14-azanonadecyl)pentanamide (compound C).—To a solution of **B** (18.0 mg, 0.031 mmol) and *N*-(13-amino-4,7,10-trioxatridecanyl)-D-biotinamide (CAS# 183896–00-6) (13.8 mg, 0.031 mmol), and HATU (23.6 mg, 0.062 mmol) in DMF (1 mL) was added DIPEA (10.4 mL, 0.062 mmol) at room temperature for 1 hour. After workup the reaction, the residue was purified by HPLC (0.1% TFA/MeCN) to afford **C** (3.5 mg, 11% yield). MS: m/z $(M+1)^+$: 1013.61.

Representative procedure for three-component reaction.

A 10 mL microwave reaction tube was charged with 4-bromopyridin-2-amine (1 mmol, 1 equiv.), aldehyde e.g. 3-(3-chloro-4-methoxyphenyl)propanal (1.2 mmol, 1.2 equiv), isocyanide e.g cyclohexylisocyanide (1 mmol, 1 equiv), and $Sc(OTf)_3$ (0.08 mmol, 0.08 equiv.) in 2 mL of 3:1 CH_2Cl_2/MeOH (Scheme 1). The reaction mixture was heated under microwave irradiation at 100 °C for 40 min. The mixture was concentrated and purified by flash chromatography eluted with 20% EtOAc in hexane to provide product as a yellow solid (95–97%).

Representative procedure for the Suzuki reaction.

To a solution of Groebke−Blackburn−Bienayme reaction adduct (1 mmol, 1 equiv.), 3,5-dimethylisoxazole-4-boronic acid pinacol ester (1.2 mmol, 1.2 equiv.), K_2CO_3 (2.0 mmol, 2.0 equiv.) and $Pd(dppf)Cl_2{\cdot}CH_2Cl_2$ (0.08 mmol, 0.08 equiv. 8% mol), in 2 mL of 2:1 DME/H_2O was heated under microwave irradiation at 120 °C for 40 min (Scheme 1). The mixture was concentrated and purified by flash chromatography eluted with 30% EtOAc in hexane to provide the desired product in 90–97% yield.

N-((3s,5s,7s)-adamantan-1-yl)-2-(4-methoxyphenyl)-5,7-dimethylimidazo[1,2-a]pyridin-3-amine (1, 91% yield).—^{1}H NMR (400 MHz, $CDCl_3$) δ 7.76 – 7.69 (m, 2H), 7.15 (s, 1H), 6.97 – 6.93 (m, 2H), 6.27 (s, 1H), 3.86 (s, 3H), 3.49 (s, 1H), 2.93 (s, 3H), 2.32 (s, 3H), 1.52 – 1.40 (m, 6H), 1.35 – 1.25 (m, 2H), 0.97 – 0.87 (m, 2H). ^{13}C NMR (101 MHz, $CDCl_3$) δ 158.76, 143.62, 136.03, 134.63, 129.72, 128.69, 116.43, 113.96, 113.60, 56.62, 55.57, 55.23, 42.97, 36.25, 29.64, 20.96, 20.89. HRMS (ESI-Orbitrap) m/z: $(M+H)^+$ Calcd for $C_{26}H_{31}N_3O$ 402.25454, found 402.2545.

N-((3s,5s,7s)-adamantan-1-yl)-7-(3,5-dimethylisoxazol-4-yl)-2-(4-methoxyphenyl)imidazo[1,2-a]pyridin-3-amine (2, 90% yield) —^{1}H NMR (400 MHz, $CDCl_3$) δ 8.31 (d, J = 8.0 Hz, 1H), 7.91 – 7.88 (m, 2H), 7.71 (dd, J = 5.8, 3.3 Hz, 1H), 7.53 (dd, J = 5.7, 3.3 Hz, 1H),

7.00 – 6.96 (m, 2H), 3.88 (s, 3H), 3.49 (s, 1H) 2.49 (s, 3H), 2.35 (s, 3H), 1.45 – 1.39 (m, 3H), 1.37 – 1.28 (m, 12H). ^{13}C NMR (101 MHz, $CDCl_3$) δ 167.76, 159.02, 158.31, 147.09, 144.52, 141.71, 139.80, 132.41, 130.88, 129.26, 128.79, 123.56, 116.50, 113.71, 112.14, 56.66, 55.25, 43.91, 38.70, 36.13, 30.34, 29.66, 28.91, 23.72, 22.99, 14.07, 11.87, 10.96. HRMS (ESI-Orbitrap) m/z: $(M+H)^+$ Calcd for $C_{29}H_{32}N_4O_2$ 469.26036, found 469.2604.

N-cyclohexyl-7-(3,5-dimethylisoxazol-4-yl)-2-(4-methoxyphenyl)imidazo[1,2-a]pyridin-3-amine (3, 89% yield).—^{1}H NMR (400 MHz, $CDCl_3$) δ 8.15 (d, J = 8.0 Hz, 1H), 8.00 (s, 1H), 7.72 (d, J = 3.3 Hz, 1H), 7.54 – 7.52 (m, 2H), 7.41 (dd, J = 1.7, 0.9 Hz, 1H), 7.03 – 6.99 (m, 2H), 3.87 (s, 3H), 3.00 (t, J = 10.2 Hz, 1H), 2.48 (s, 3H), 2.35 (s, 3H), 1.68 (dd, J = 12.2, 6.1 Hz, 4H), 1.46 – 1.39 (m, 6H). ^{13}C NMR (101 MHz, $CDCl_3$) δ 167.75, 165.76, 158.55, 144.63, 141.26, 132.40, 130.87, 128.77, 128.26, 124.30, 122.69, 116.62, 113.99, 112.47, 56.95, 55.27, 38.69, 30.32, 28.90, 23.71, 22.97, 14.05, 10.95. HRMS (ESI-Orbitrap) m/z: $(M+H)^+$ Calcd for $C_{25}H_{28}N_4O_2$ 417.22907, found 417.2291.

2-(4-methoxyphenyl)-5,7-dimethyl-N-(2,4,4-trimethylpentan-2-yl)imidazo[1,2-a]pyridin-3-amine (5, 92% yield).—^{1}H NMR (400 MHz, $CDCl_3$) δ 7.70 – 7.68 (m, 1H), 7.67 (d, J = 2.2 Hz, 1H), 7.15 (s, 1H), 6.98 – 6.95 (m, 2H), 6.28 (s, 1H), 3.85 (s, 3H), 3.49 (s, 1H), 2.91 (s, 3H), 2.31 (s, 3H), 1.45 (s, 2H), 0.95 (s, 9H), 0.77 (s, 6H). ^{13}C NMR (101 MHz, $CDCl_3$) δ 158.88, 143.68, 135.93, 134.64, 130.86, 129.87, 128.77, 124.29, 116.44, 113.68, 60.55, 56.22, 55.26, 31.83, 30.33, 28.33, 22.98, 20.77, 14.05. HRMS (ESI-Orbitrap) m/z: $(M+H)^+$ Calcd for $C_{24}H_{33}N_3O$ 380.27019, found 380.2702.

N-cyclohexyl-7-(3,5-dimethylisoxazol-4-yl)-2-phenethylimidazo[1,2-a]pyridin-3-amine (7, 88% yield).—^{1}H NMR (400 MHz, $CDCl_3$) δ 8.22 (dd, J = 7.1, 0.9 Hz, 1H), 7.37 (dd, J = 1.7, 0.9 Hz, 1H), 7.29 (dd, J = 7.9, 6.7 Hz, 2H), 7.23 – 7.19 (m, 3H), 6.64 (dd, J = 7.1, 1.7 Hz, 1H), 3.14 – 3.04 (m, 4H), 3.50 (1H), 2.48 (s, 3H), 2.35 (s, 3H), 1.66 (d, J = 2.8 Hz, 6H), 1.59 (d, J = 22.3 Hz, 4H), 0.91 (dt, J = 9.7, 7.3 Hz, 1H). ^{13}C NMR (101 MHz, $CDCl_3$) δ 165.70, 158.51, 142.13, 141.76, 141.19, 128.57, 128.41, 125.98, 125.67, 123.53, 122.93, 116.10, 115.25, 111.80, 68.12, 55.40, 43.90, 36.17, 30.39, 29.64, 24.86, 11.84, 11.04. HRMS (ESI-Orbitrap) m/z: $(M+H)^+$ Calcd for $C_{26}H_{30}N_4O$ 415.2480, found 415.2499.

N-((3s,5s,7s)-adamantan-1-yl)-7-(3,5-dimethylisoxazol-4-yl)-2-phenethylimidazo[1,2-a]pyridin-3-amine (8, 90% yield).—^{1}H NMR (400 MHz, $CDCl_3$) δ 8.04 (d, J = 7.9 Hz, 1H), 7.71 (dd, J = 5.7, 3.3 Hz, 1H), 7.39 (s, 1H), 7.29 (d, J = 6.8 Hz, 1H), 7.24 – 7.18 (m, 3H), 6.66 (dd, J = 7.0, 1.7 Hz, 1H), 3.09 (d, J = 7.0 Hz, 2H), 3.07 – 3.02 (m, 2H), 2.71 (s, 1H), 2.47 (s, 3H), 2.34 (s, 3H), 1.74 (dd, J = 22.8, 7.9 Hz, 4H), 1.45 – 1.30 (m, 6H), 1.15 (t, J = 10.1 Hz, 5H). ^{13}C NMR (101 MHz, $CDCl_3$) δ 165.71, 158.51, 142.03, 141.17, 139.08, 132.40, 130.86, 128.77, 128.59, 128.41, 126.03, 125.54, 122.62, 116.32, 112.25, 57.15, 38.69, 35.84, 34.19, 29.93, 28.90, 25.70, 24.81, 22.97, 14.05, 11.00. HRMS (ESI-Orbitrap) m/z: $(M+H)^+$ Calcd for $C_{30}H_{34}N_4O$ 467.28109, found 467.2811.

7-(3,5-dimethylisoxazol-4-yl)-2-phenethyl-N-(2,4,4-trimethylpentan-2-yl)imidazo[1,2-a]pyridin-3-amine (12, 89%).—^{1}H NMR (400

MHz, $CDCl_3$) δ 8.17 (dd, J = 7.1, 1.0 Hz, 1H), 7.36 (dd, J = 1.7, 0.9 Hz, 1H), 7.32 – 7.27 (m, 2H), 7.24 – 7.17 (m, 3H), 6.65 (dd, J = 7.1, 1.7 Hz, 1H), 3.49 (s, 1H), 3.13 – 3.05 (m, 4H), 2.48 (s, 3H), 2.34 (s, 3H), 1.59 (s, 2H), 1.14 (s, 6H), 1.07 (s, 9H). ^{13}C NMR (101 MHz, $CDCl_3$) δ 165.72, 158.52, 142.09, 141.86, 141.32, 128.53, 128.44, 126.02, 125.72, 123.51, 116.21, 115.23, 111.86, 59.50, 56.77, 35.84, 31.94, 31.78, 30.54, 29.22, 11.84, 11.04. HRMS (ESI-Orbitrap) m/z: $(M+H)^+$ Calcd for $C_{28}H_{36}N_4O$ 445.29674, found 445.2967.

N-(tert-butyl)-7-(3,5-dimethylisoxazol-4-yl)-2-phenethylimidazo[1,2-a]pyridin-3-amine (13, 89% yield).—^{1}H NMR (400 MHz, $CDCl_3$) δ 8.17 (dd, J = 7.1, 1.0 Hz, 1H), 7.37 (dd, J = 1.7, 0.9 Hz, 1H), 7.31 – 7.27 (m, 2H), 7.22 – 7.18 (m, 3H), 6.64 (dd, J = 7.1, 1.7 Hz, 1H), 3.49 (s, 1H), 3.10 – 3.07 (m, 4H), 2.48 (s, 3H), 2.34 (s, 3H), 1.15 (s, 9H). ^{13}C NMR (101 MHz, $CDCl_3$) δ 165.73, 158.51, 142.09, 141.81, 141.11, 128.55, 128.44, 126.01, 125.80, 123.44, 116.18, 111.88, 110.78, 55.37, 35.82, 30.94, 30.29, 24.85, 11.83, 11.03. HRMS (ESI-Orbitrap) m/z: $(M+H)^+$ Calcd for $C_{24}H_{28}N_4O$ 389.24415, found 389.2441.

N-((3s,5s,7s)-adamantan-1-yl)-7-(3,5-dimethylisoxazol-4-yl)-2-(4-methoxyphenethyl)imidazo[1,2-a]pyridin-3-amine (14, 87% yield).—^{1}H NMR (400 MHz, $CDCl_3$) δ 8.23 (dd, J = 7.1, 0.9 Hz, 1H), 7.36 (dd, J = 1.8, 1.0 Hz, 1H), 7.14 – 7.10 (m, 2H), 6.85 – 6.81 (m, 2H), 6.64 (dd, J = 7.1, 1.7 Hz, 1H), 3.79 (s, 3H), 3.50 (s, 1H), 3.04 (td, J = 3.2, 1.8 Hz, 4H), 2.48 (s, 3H), 2.35 (s, 3H), 1.67 – 1.58 (m, 15H). ^{13}C NMR (101 MHz, $CDCl_3$) δ 158.54, 157.88, 134.22, 129.48, 123.54, 116.11, 113.83, 111.82, 55.44, 55.29, 43.92, 43.87, 36.18, 34.88, 30.62, 29.66, 11.87, 11.07. HRMS (ESI-Orbitrap) m/z: $(M+H)^+$ Calcd for $C_{31}H_{36}N_4O_2$ 497.29166, found 497.2917.

N-cyclohexyl-7-(3,5-dimethylisoxazol-4-yl)-2-(4-methoxyphenethyl)imidazo[1,2-a]pyridin-3-amine (16, 90% yield).—^{1}H NMR (400 MHz, $CDCl_3$) δ 8.04 (dd, J = 7.0, 0.9 Hz, 1H), 7.36 (dd, J = 1.7, 0.9 Hz, 1H), 7.13 – 7.09 (m, 2H), 6.85 – 6.81 (m, 2H), 6.65 (dd, J = 7.0, 1.7 Hz, 1H), 3.79 (s, 3H), 3.49 (s, 1H), 3.02 (dtd, J = 11.8, 5.9, 1.7 Hz, 4H), 2.47 (s, 3H), 2.34 (s, 3H), 1.81 – 1.66 (m, 5H), 1.27 – 1.09 (m, 6H). ^{13}C NMR (101 MHz, $CDCl_3$) δ 165.68, 158.53, 157.89, 141.21, 139.34, 134.13, 129.47, 125.36, 122.62, 116.37, 115.31, 113.81, 112.15, 57.20, 55.26, 34.91, 34.22, 30.21, 25.72, 24.83, 11.81, 11.01. HRMS (ESI-Orbitrap) m/z: $(M+H)^+$ Calcd for $C_{27}H_{32}N_4O_2$ 445.26036, found 445.2605.

7-(3,5-dimethylisoxazol-4-yl)-N-isopropyl-2-(4-methoxyphenethyl)imidazo[1,2-a]pyridin-3-amine (17, 88% yield).—^{1}H NMR (400 MHz, $CDCl_3$) δ 8.25 (d, J = 7.1 Hz, 1H), 8.16 (s, 1H), 7.11 (dd, J = 7.0, 1.3 Hz, 1H), 7.08 – 7.04 (m, 2H), 6.83 – 6.79 (m, 2H), 4.27 – 4.15 (m, 1H), 3.78 (s, 3H), 3.49 (s, 1H), 3.15 (q, J = 8.2, 7.6 Hz, 2H), 3.09 (dd, J = 9.6, 6.4 Hz, 2H), 2.55 (s, 3H), 2.38 (s, 3H), 1.05 (s, 3H), 1.03 (s, 3H). ^{13}C NMR (101 MHz, $CDCl_3$) δ 167.47, 158.35, 157.86, 137.33, 133.98, 132.14, 129.59, 126.49, 123.42, 116.40, 114.13, 113.52, 112.59, 55.32, 49.71, 38.68, 33.93, 27.25, 23.22, 12.12, 11.09. HRMS (ESI-Orbitrap) m/z: $(M+H)^+$ Calcd for $C_{24}H_{28}N_4O_2$ 405.22907, found 405.2291.

N-cyclohexyl-7-(3,5-dimethylisoxazol-4-yl)-2-(4-ethoxyphenethyl)imidazo[1,2-a]pyridin-3-amine (19, 90% yield).—^{1}H NMR (400 MHz, $CDCl_3$) δ 8.05 (dd, J = 7.0, 1.0 Hz, 1H), 7.37 (dd, J = 1.7, 0.9 Hz, 1H), 7.11 – 7.07 (m, 2H),

6.83 – 6.78 (m, 2H), 6.66 (dd, J = 7.0, 1.7 Hz, 1H), 4.01 (q, J = 7.0 Hz, 2H), 3.49 (s, 1H), 3.07 – 2.97 (m, 4H), 2.74 – 2.62 (m, 1H), 2.47 (s, 3H), 2.34 (s, 3H), 1.80 – 1.68 (m, 4H), 1.40 (t, J = 7.0 Hz, 3H), 1.26 – 1.12 (m, 6H). ^{13}C NMR (101 MHz, $CDCl_3$) δ 165.68, 158.51, 157.24, 141.16, 139.26, 133.95, 129.44, 125.41, 125.39, 122.62, 116.31, 115.29, 114.41, 112.18, 63.39, 57.19, 34.92, 34.20, 30.16, 25.71, 24.81, 14.88, 11.80, 11.00. HRMS (ESI-Orbitrap) m/z: $(M+H)^+$ Calcd for $C_{28}H_{34}N_4O_2$ 459.27601, found 459.2760.

2-(3-chloro-4-methoxyphenethyl)-N-cyclohexyl-7-(3,5-dimethylisoxazol-4-yl)imidazo[1,2-a]pyridin-3-amine (23, 90% yield).—^{1}H NMR (400 MHz, $CDCl_3$) δ 8.05 (dd, J = 7.0, 1.0 Hz, 1H), 7.36 (dd, J = 1.7, 0.9 Hz, 1H), 7.23 (d, J = 2.2 Hz, 1H), 7.04 (dd, J = 8.3, 2.2 Hz, 1H), 6.83 (d, J = 8.4 Hz, 1H), 6.66 (dd, J = 7.0, 1.7 Hz, 1H), 3.87 (s, 3H), 3.49 (s, 1H), 3.08 – 2.97 (m, 4H), 2.66 – 2.52 (m, 1H), 2.48 (s, 3H), 2.34 (s, 3H), 1.80 – 1.69 (m, 4H), 1.28 – 1.11 (m, 6H). ^{13}C NMR (101 MHz, $CDCl_3$) δ 165.70, 158.50, 153.24, 141.27, 138.97, 135.23, 130.19, 127.75, 125.53, 122.64, 122.07, 116.37, 115.27, 112.23, 112.00, 57.24, 56.15, 34.47, 34.23, 29.74, 25.70, 24.81, 11.80, 11.00. HRMS (ESI-Orbitrap) m/z: $(M+H)^+$ Calcd for $C_{27}H_{31}N_4O_2Cl$ 479.22139, found 479.2216.

N-cyclohexyl-7-(3,5-dimethylisoxazol-4-yl)-2-(3-(4-methoxyphenyl)propyl)imidazo[1,2-a]pyridin-3-amine (25, 89% yield).—^{1}H NMR (400 MHz, $CDCl_3$) δ 8.06 (dd, J = 7.0, 1.0 Hz, 1H), 7.35 (dd, J = 1.7, 0.9 Hz, 1H), 7.15 – 7.11 (m, 2H), 6.86 – 6.81 (m, 2H), 6.66 (dd, J = 7.0, 1.7 Hz, 1H), 3.79 (s, 3H), 3.49 (s, 1H), 2.79 (q, J = 4.0, 3.5 Hz, 1H), 2.76 – 2.70 (m, 2H), 2.67 (t, J = 7.5 Hz, 2H), 2.46 (s, 3H), 2.32 (s, 3H), 2.11 (tt, J = 8.8, 6.8 Hz, 2H), 1.84 – 1.71 (m, 4H), 1.24 (s, 2H), 1.20 – 1.14 (m, 4H). ^{13}C NMR (101 MHz, $CDCl_3$) δ 165.69, 158.54, 157.71, 141.17, 139.92, 134.13, 129.37, 125.31, 124.95, 122.53, 116.39, 115.33, 113.70, 112.20, 57.21, 55.26, 34.57, 34.22, 30.94, 26.46, 25.74, 24.85, 11.78, 10.99. HRMS (ESI-Orbitrap) m/z: $(M+H)^+$ Calcd for $C_{28}H_{34}N_4O_2$ 459.27601, found 459.2761.

7-(3,5-dimethylisoxazol-4-yl)-2-(4-methoxyphenethyl)-N-(2,4,4-trimethylpentan-2-yl)imidazo[1,2-a]pyridin-3-amine (26, 91% yield).—^{1}H NMR (400 MHz, $CDCl_3$) δ 8.18 (d, J = 7.0 Hz, 1H), 7.38 (s, 1H), 7.11 – 7.07 (m, 2H), 6.85 – 6.80 (m, 2H), 6.65 (dd, J = 7.1, 1.6 Hz, 1H), 3.79 (s, 3H), 3.04 (s, 3H), 2.48 (s, 3H), 2.46 – 2.35 (m, 1H), 2.35 (s, 3H), 2.32 – 2.20 (m, 1H), 1.25 (s, 2H), 1.14 (s, 6H), 1.08 (s, 9H). ^{13}C NMR (101 MHz, $CDCl_3$) δ ^{13}C NMR (101 MHz, cdcl$_3$) δ 165.74, 158.50, 157.87, 134.08, 129.43, 123.83, 123.51, 116.11, 115.20, 113.82, 111.92, 59.50, 56.77, 55.21, 34.92, 31.93, 31.86, 31.77, 30.73, 29.23, 24.85, 11.85, 11.04. HRMS (ESI-Orbitrap) m/z: $(M+H)^+$ Calcd for $C_{29}H_{38}N_4O_2$ 475.30732, found 475.3073.

7-(3,5-dimethylisoxazol-4-yl)-2-(4-ethoxyphenethyl)-N-(2,4,4-trimethylpentan-2-yl)imidazo[1,2-a]pyridin-3-amine (27, 90% yield).—^{1}H NMR (400 MHz, $CDCl_3$) δ 8.17 (dd, J = 7.1, 0.9 Hz, 1H), 7.37 (dd, J = 1.7, 0.9 Hz, 1H), 7.12 – 7.03 (m, 2H), 6.86 – 6.77 (m, 2H), 6.65 (dd, J = 7.1, 1.7 Hz, 1H), 4.01 (q, J = 6.9 Hz, 2H), 3.49 (s, 1H), 3.03 (s, 4H), 2.48 (s, 3H), 2.34 (s, 3H), 1.58 (s, 2H), 1.41 (t, J = 7.0 Hz, 3H), 1.13 (s, 6H), 1.07 (s, 9H). ^{13}C NMR (101 MHz, $CDCl_3$) δ 165.75, 158.53, 157.26, 141.77, 133.95, 129.43, 123.87, 123.53, 116.13, 115.22, 114.42, 111.91, 63.36, 59.51, 56.78, 34.96, 31.94,

31.79, 30.77, 29.24, 14.90, 11.86, 11.05. HRMS (ESI-Orbitrap) m/z: $(M+H)^+$ Calcd for $C_{30}H_{40}N_4O_2$ 489.32297, found 489.3228.

7-(3,5-dimethylisoxazol-4-yl)-2-(4-isopropoxyphenethyl)-N-(2,4,4-trimethylpentan-2-yl)imidazo[1,2-a]pyridin-3-amine (28, 89% yield).—^{1}H NMR (400 MHz, $CDCl_3$) δ 8.17 (dd, J = 7.0, 1.0 Hz, 1H), 7.38 (dd, J = 1.7, 0.9 Hz, 1H), 7.08 – 7.04 (m, 2H), 6.82 – 6.78 (m, 2H), 6.65 (dd, J = 7.1, 1.7 Hz, 1H), 4.50 (p, J = 6.1 Hz, 1H), 3.49 (s, 1H), 3.03 (d, J = 2.0 Hz, 4H), 2.48 (s, 3H), 2.34 (s, 3H), 1.59 (s, 2H), 1.33 (d, J = 6.1 Hz, 6H), 1.13 (s, 6H), 1.07 (s, 9H). ^{13}C NMR (101 MHz, $CDCl_3$) δ 165.74, 158.52, 156.16, 141.79, 141.27, 133.91, 129.44, 125.77, 123.85, 123.52, 116.12, 115.82, 115.23, 111.89, 75.00, 69.80, 59.49, 56.79, 34.96, 31.94, 31.77, 30.70, 29.21, 24.86, 22.10, 11.85, 11.04. HRMS (ESI-Orbitrap) m/z: $(M+H)^+$ Calcd for $C_{31}H_{42}N_4O_2$ 503.33862, found 503.3388.

2-(3-chloro-4-ethoxyphenethyl)-N-cyclohexyl-7-(3,5-dimethylisoxazol-4-yl)imidazo[1,2-a]pyridin-3-amine (29, 91% yield).—^{1}H NMR (400 MHz, $CDCl_3$) δ 8.05 (dd, J = 7.1, 1.0 Hz, 1H), 7.36 (dd, J = 1.7, 0.9 Hz, 1H), 7.22 (d, J = 2.2 Hz, 1H), 7.01 (dd, J = 8.3, 2.2 Hz, 1H), 6.82 (d, J = 8.4 Hz, 1H), 6.66 (dd, J = 7.0, 1.7 Hz, 1H), 4.08 (q, J = 7.0 Hz, 2H), 3.49 (s, 1H), 3.07 – 2.96 (m, 4H), 2.53 (d, J = 14.2 Hz, 1H), 2.48 (s, 3H), 2.34 (s, 3H), 1.82 – 1.69 (m, 4H), 1.45 (t, J = 7.0 Hz, 3H), 1.32 – 1.04 (m, 6H). ^{13}C NMR (101 MHz, $CDCl_3$) δ 165.71, 158.52, 152.70, 141.28, 139.04, 135.15, 130.19, 127.68, 125.50, 125.31, 122.65, 122.57, 116.40, 115.30, 113.44, 112.23, 64.80, 57.25, 34.54, 34.25, 29.78, 25.73, 24.83, 14.77, 11.82, 11.02. HRMS (ESI-Orbitrap) m/z: $(M+H)^+$ Calcd for $C_{28}H_{33}N_4O_2Cl$ 493.23704, found 493.2371.

2-(3-(3-chloro-4-methoxyphenyl)propyl)-N-cyclohexyl-7-(3,5-dimethylisoxazol-4-yl)imidazo[1,2-a]pyridin-3-amine (30, 90% yield).—^{1}H NMR (400 MHz, $CDCl_3$) δ 8.07 (dd, J = 7.0, 1.0 Hz, 1H), 7.34 (s, 1H), 7.22 (d, J = 2.1 Hz, 1H), 7.07 (dd, J = 8.4, 2.1 Hz, 1H), 6.85 (d, J = 8.4 Hz, 1H), 6.66 (dd, J = 7.0, 1.6 Hz, 1H), 3.88 (s, 3H), 3.49 (s, 1H), 2.74 (d, J = 7.4 Hz, 2H), 2.65 (t, J = 7.5 Hz, 2H), 2.46 (s, 3H), 2.45 – 2.40 (m, 1H), 2.32 (s, 3H), 2.11 (q, J = 7.8 Hz, 2H), 1.46 – 1.25 (m, 4H), 1.23 – 1.14 (m, 6H). ^{13}C NMR (101 MHz, $CDCl_3$) δ 165.68, 158.53, 153.08, 141.23, 139.82, 135.33, 130.19, 127.61, 125.34, 124.91, 122.54, 122.03, 116.44, 115.33, 112.22, 111.98, 106.09, 57.19, 56.19, 34.37, 34.27, 30.75, 26.46, 25.74, 24.86, 11.79, 10.99. HRMS (ESI-Orbitrap) m/z: $(M+H)^+$ Calcd for $C_{28}H_{33}N_4O_2Cl$ 493.23704, found 493.2370.

2-(3-chloro-4-ethoxyphenethyl)-7-(3,5-dimethylisoxazol-4-yl)-N-(2,4,4-trimethylpentan-2-yl)imidazo[1,2-a]pyridin-3-amine (31, 91% yield).—^{1}H NMR (400 MHz, $CDCl_3$) δ 8.18 (dd, J = 7.1, 1.0 Hz, 1H), 7.35 (dd, J = 1.6, 0.9 Hz, 1H), 7.20 (d, J = 2.1 Hz, 1H), 6.98 (dd, J = 8.3, 2.2 Hz, 1H), 6.81 (d, J = 8.4 Hz, 1H), 6.65 (dd, J = 7.1, 1.7 Hz, 1H), 4.08 (q, J = 7.0 Hz, 2H), 3.35 (s, 1H), 3.03 (s, 4H), 2.48 (s, 3H), 2.46 – 2.36 (m, 1H), 2.34 (s, 3H), 1.61 (s, 2H), 1.46 (t, J = 7.0 Hz, 3H), 1.14 (s, 6H), 1.09 (s, 9H). ^{13}C NMR (101 MHz, $CDCl_3$) δ 165.74, 158.51, 152.69, 141.88, 141.04, 135.13, 130.16, 127.60, 125.83, 123.79, 123.52, 122.58, 116.20, 115.22, 113.41, 111.93, 64.76, 59.56, 56.82, 34.58, 31.94, 31.80, 30.41, 29.26, 14.77, 11.85, 11.04. HRMS (ESI-Orbitrap) m/z: $(M+H)^+$ Calcd for $C_{30}H_{40}N_4O_2Cl$ 524.29182, found 524.2918.

2-(3,4-dimethoxyphenethyl)-7-(3,5-dimethylisoxazol-4-yl)-N-isopropylimidazo[1,2-a]pyridin-3-amine (33, 92% yield)..—^{1}H NMR (400 MHz, $CDCl_3$) δ 8.06 (d, J = 7.0 Hz, 1H), 7.38 (s, 1H), 6.78 (q, J = 8.2 Hz, 2H), 6.67 (d, J = 11.2 Hz, 2H), 4.22 (t, J = 6.0 Hz, 1H), 3.86 (s, 3H), 3.77 (s, 3H), 3.49 (s, 1H) 3.18 (h, J = 6.1 Hz, 2H), 2.47 (s, 3H), 2.33 (s, 3H), 1.48 – 1.37 (m, 2H), 1.06 (d, J = 6.3 Hz, 6H). ^{13}C NMR (101 MHz, $CDCl_3$) δ 167.75, 165.70, 158.49, 148.73, 147.29, 141.27, 139.51, 134.63, 130.88, 128.78, 125.56, 122.61, 120.25, 116.32, 111.96, 111.20, 55.95, 55.71, 49.62, 38.70, 30.34, 28.91, 23.45, 14.06, 10.96. HRMS (ESI-Orbitrap) m/z: $(M+H)^+$ Calcd for $C_{25}H_{30}N_4O_3$ 435.23964, found 435.2397.

7-(3,5-dimethylisoxazol-4-yl)-2-(3-(4-methoxyphenyl)propyl)-N-(2,4,4-trimethylpentan-2-yl)imidazo[1,2-a]pyridin-3-amine (34, 91% yield).—^{1}H NMR (400 MHz, $CDCl_3$) δ 8.23 (d, J = 7.1 Hz, 1H), 8.10 (s, 2H), 7.11 (d, J = 8.5 Hz, 2H), 6.82 (d, J = 8.6 Hz, 2H), 3.78 (s, 3H), 3.49 (s, 1H), 2.76 (dd, J = 8.8, 6.6 Hz, 2H), 2.65 (t, J = 7.2 Hz, 2H), 2.48 (s, 3H), 2.34 (s, 3H), 2.15 (p, J = 7.5 Hz, 2H), 1.61 (s, 2H), 1.11 (s, 6H), 1.08 (s, 9H). ^{13}C NMR (101 MHz, $CDCl_3$) δ 167.76, 165.96, 157.73, 134.21, 133.85, 132.42, 130.89, 129.48, 129.37, 128.79, 123.51, 113.72, 67.75, 59.68, 56.77, 38.88, 38.70, 31.92, 31.78, 30.56, 29.14, 23.97, 22.97, 14.07, 11.10. HRMS (ESI-Orbitrap) m/z: $(M+H)^+$ Calcd for $C_{30}H_{40}N_4O_2$ 489.32297, found 489.3229.

BRD4 AlphaScreen Assay.

BRD4 (BD1) assays were performed with minimal modifications from the manufacturer's protocol (PerkinElmer, USA). All reagents were diluted in 50 mM HEPES, 150 mM NaCl, 0.1% w/v BSA, 0.01% w/v Tween20, pH 7.5 and allowed to equilibrate to room temperature prior to addition to plates. After the addition of Alpha beads to master solutions, all subsequent steps were performed under low light conditions. A 2x solution of components with final concentrations of His-BRD4 at 40 nM, Ni-coated Acceptor Beads at 25 μg/ml, and 20 nM biotinylated-JQ1(S) was added in 10 μL to 384-well plates (AlphaPlate-384, PerkinElmer, USA). Plates were spun down at 150g, after which 100 nL of compound in DMSO from stock plates were added by pin transfer using a Janus Workstation (PerkinElmer, USA). The streptavidin-coated donor beads (25 μg/ml final) were added in the same manner as the previous solution, in a 2x solution of 10 μL volume. Following this addition, plates were sealed with foil to prevent light exposure and evaporation. The plates were spun down again at 150g. Plates were incubated at room temperature for 1 hour and then read on an Envision 2104 (PerkinElmer, USA) using the manufacturer's protocol.

BRD4(1) and CBP AlphaScreen Assay.

Assays were performed with minor modifications from the manufacturer's protocol (Perkin Elmer, USA). All reagents were diluted in AlphaScreen™ buffer (50 mM HEPES, 150 mM NaCl, 0.01% v/v Tween-20, 0.1% w/v BSA, pH 7.4). After addition of Alpha beads to master solutions, all subsequent steps were performed under low light conditions. A 2x solution of components with final concentrations of His-BRD4(1) at 20 nM or His-CBP at 50 nM, Ni-coated acceptor bead at 10 μg/ml, biotinylated-JQ at 10 nM or biotinylated peptide at 100 nM or Compound C at 10nM was added in 10 μL to 384-well plates (AlphaPlate-384, PerkinElmer) using an EL406 liquid handler (Biotek, USA). Plates were

spun down at 1000 rpm. A 10-point 1:$\sqrt{sqrt(10)}$ serial dilution of compounds in DMSO was prepared at 200x the final concentration. 100 nL of compound from these stock plates were added by pin transfer using a Janus Workstation (PerkinElmer). A 2x solution of streptavidin-coated donor beads with a final concentration of 10 μg/ml was added in a 10 μL volume. The plates were spun down again at 1000 rpm and sealed with foil to prevent light exposure and evaporation. The plates were then incubated at room temperature for 1 hour and read on an Envision 2104 (PerkinElmer) using the manufacturer's protocol. IC_{50} values were calculated using a 4-parameter logistic curve in Prism 6 (GraphPad Software, USA) after normalization to DMSO-treated negative control wells.

The profiling data and the Kd data are generated by Eurofins using BromoMAX^{SM} and BromoKdELECT^{SM} services.

Molecular Docking Experiments.

All steps for the docking experiments in this study were performed using the Schrödinger 2018–3 suite (Small-Molecule Drug Discovery Suite 2018–3: Maestro, Schrödinger, LLC, New York, NY, 2018). CBP (PDB ID: 4NR7) and BRD4 (PDB ID: 5BT4) were first processed in order to extract individual protein chains and remove the co-crystallized ligand using the *split_structures.py* command lines, while keeping all crystal waters. Both structures were processed using the protein prep wizard command line.[29,30] This step adds hydrogen atoms, assigns bonds orders using CCD, caps termini, assigns protonation states using PROPKA with pH of 7, optimizes hydrogen bonds, and runs a restrained minimization of the full protein. The receptor grids were then generated for a 25 Å x 25 Å x 25 Å outer box and 15 Å x 15 Å x 15 Å inner box centered at the centroid of pocket residues 6 Å away from the protein's respective co-crystallized ligand. CBP's pocket includes residues 1106, 1109–1111, 1113, 1115, 1120, 1122, 1125, 1164, 1167, 1168, 1173, 1174, and 1177; and BRD4's pocket includes residues 79–89, 91, 92, 94, 97, 101, 105, 106, 132, 133, 135–140, 144, 145–147, 149, and 150. Smiles strings of compounds **3**, **4**, **7**, **16**, **23**, and CBP30 were generated using BindingDB[39] molecular drawing tool. All molecules were converted to mae files using *structconvert* command and processed using the *ligprep* command in order to add explicit hydrogen atoms using Schrödinger 2018–3 suite. All generated ligands were docked into the pockets of both receptors using Glide with extra precision docking and default parameters to generate 10 poses for each ligand-receptor complex. The top poses from each ligand were selected for analysis. The PDBs were chosen because their co-crystallized ligands were from the same chemical series and the top poses have resulted in very similar binding modes of the shared chemical moiety. As mentioned in the methods section, PDB codes 4NR7 and 5BT4 were used for CBP and BRD4, respectively. We have also added the PDB codes to the figure legends for further clarity. Figure 6 shows molecular graphics of the co-crystallized PDBs 4NR7 and 5BT4.

Protein expression and purification.

The expression plasmid for CBP BRD was purchased from Addgene (#38977) and transformed into *E. coli* BL21 (DE3)-RIL cells, grown at 37 °C in LB medium (Fisher Scientific) containing carbenicillin and chloramphenicol. At OD600 of 0.6, the culture was cooled down to 18 °C and induced with 0.1 mM IPTG. After 18 h growth, the culture

was harvested by centrifugation at 6,000 × g for 25 min and stored at −80 °C. Harvested cell pellet was re-suspended in 50 mM Na/K phosphate buffer (pH 7.4) containing 100 mM NaCl, 40 mM imidazole, 0.01% w/v lysozyme and 0.01% v/v Triton X-100 at 4 °C for 1 h, subjected to sonication and the lysate was clarified by centrifugation (30,000 × g for 45 min at 4 °C). CBP BRD was purified by FPLC at 4 °C using columns and chromatography materials from GE Healthcare. The lysate was subjected to an immobilized Ni2+ affinity chromatography column equilibrated with 50 mM Na/K phosphate buffer (pH 7.4) containing 100 mM NaCl and 40 mM imidazole using a gradient from 40 to 500 mM of imidazole. Fractions containing the target protein were combined and incubated overnight with TEV protease at 4 °C, and the cleaved His6-tag was removed by a second Ni2+ affinity column. CBP was purified to homogeneity by size exclusion chromatography using Superdex 75 in elution buffer 50 mM HEPES/100 mM NaCl/1 mM DTT (pH 7.5). CBP BRD eluted as a monomer and was of crystallization grade quality (> 95% purity as judged by SDS-PAGE). Protein was concentrated to 11 mg/ml, aliquots were flash-frozen in liquid N_2 and stored at −80 °C

Crystallization and X-ray crystallography.

Crystallization experiments were performed at 19 °C. Purified cleaved CBP BRD was subjected to screening campaigns across different precipitants using a mosquito crystallization robot (TP Labtech) in 96-well sitting drop iQ plates. CBP (10 mg/ml) was incubated with 2 mM UMB289 and 5% DMSO on ice for 30 min prior to addition of precipitant in ratios 1:2, 1:1 and 2:1 per condition. X-ray grade crystals grew from 0.1 M BIS-TRIS pH 5.5, 25% w/v polyethylene glycol 3,350. For data collection, crystals were cryoprotected using precipitant supplemented with 25% ethylene glycol and flash frozen in liquid nitrogen. X-ray diffraction data were collected at −180 °C using beamline GMCA 23ID-D of the Advanced Photon Source at Argonne National Laboratories. Data were reduced and scaled with XDS[40]. PHASER[41] was employed for molecular replacement using PDB entry 4NR7 as the search model. Refinement was carried out with PHENIX[41] and model building was performed with Coot.[42] The initial inhibitor model was generated with ligand restraints from eLBOW of the PHENIX suite. Figures were prepared using PyMOL (Schrödinger). Data collection and refinement statistics are shown in Supplementary Table S2. The coordinates and structure factors of the CBP-UMB298 (compound **23**) complex have been deposited in the PDB (accession code 7KPY).

Western Blots.

MOLM13 cells were seeded in 6-well plates at 1×10^6 cells/well, and treated with DMSO, 3.0 μM CBP30 or 3.0 μM compound **23** for 2 h. Total protein was extracted from cells using RIPA buffer (Abcam) supplemented with Halt Protease Inhibitor Cocktail (Millipore-Sigma). Samples were loaded to Invitrogen Bolt Bis-Tris Plus gels (ThermoFisher Scientific) and transferred to Invitrolon PVDF membranes (ThermoFisher Scientific) using Invitrogen Bolt wet-gel Transfer Device. Immunodetection were performed with standard techniques. The following primary and secondary antibodies were used: anti-MYC, β-actin, H3(Cell Signaling Technology), anti-H3K27ac (abcam), IRDye secondary antibodies at the concentration recommended by the manufacturer.

Real-time qPCR:

Cells were treated with DMSO, 3.0 μM CBP30 or 3.0 μM compound **23** for 2 h, and total RNA was isolated using the RNeasy kit (Qiagen). Three biological replicates were performed for each condition. cDNA was synthesized using the Tetro cDNA Synthesis Kit (Thomas Scientific) and real-time qPCR was performed using the PowerUp SYBR Green Master Mix (Life Technologies) on Applied Biosystems ViiA™ 7 Real-Time PCR System (Applied Biosystems). The following primers were utilized: MYC.F 5′GGCTCCTGGCAAAAGGTCA, MYC.R 5′CTGCGTAGTTGTGCTGATGT, GAPDH.F 5′CTGGGCTACACTGAGCACCand GAPDH.R 5′AAGTGGTCGTTGAGGGCAATG. Reactions were carried out in triplicate and expression levels normalized to GAPDH.

Cell viability.

Cells were seeded in 384-well plates (ThermoFisher Scientific) at 500 cells/well, and transfer of serial pre-diluted compounds (100 nl) was performed using a Janus Workstation (PerkinElmer). CellTiter-Glo Luminescent cell viability assay was used to determine the cell viability. Luminescent signals were read on 2104 EnVision Multilabel Plate Readers (PerkinElmer) after 5-day incubation. Data were normalized to the DMSO control, and the IC50 values were determined via nonlinear regression curve fit using GraphPad Prism 9.

Statistical analysis.

Prism 9 software was used to process the data. Student's t test was applied to compare compound-induced changes to respective controls. A P value of less than 0.05 was chosen as a threshold for statistical significance.

Supplementary Material

Refer to Web version on PubMed Central for supplementary material.

ACKNOWLEDGEMENTS

We acknowledge undergraduate student Francesca Corsini for her assistance on compound synthesis and Dr. Jason Evans for HRMS analysis of some samples. We also thank Eurofins for their expedite service on the Kd and selectivity evaluation. This work was supported by National Institutes of Health U54 grant CA156732 (W.Z.), National Cancer Institute (NCI) grants P01-CA066996–19, U54HD093540–03, P50-CA100707–15 (J.Q.) and P30-CA076292 (E.S.), and Alex's Lemonade Stand Foundation Innovation Award (J.Q.)

ABBREVIATIONS USED

BET	bromodomain and extra-terminal domain
BRD4	bromodomain 4
CREBBP or CBP	cyclic AMP response element binding protein binding protein
DSF	differential scanning fluorometry
EP300 or P300	E1A binding protein P300

MCR	multicomponent reaction
SAR	structure-activity relationship
SGC	structural genomics consortium

REFERENCES

1. Clegg MA; Tomkinson NCO; Prinjha RK; Humphreys PG Advancements in the development of non-BET bromodomain chemical probes. ChemMedChem. 2019, 14, 362–385. [PubMed: 30624862]
2. Theodoulou NH; Tomkinson NC; Prinjha RK; Humphreys PG Clinical progress and pharmacology of small molecule bromodomain inhibitors. Curr Opin Chem Biol. 2016, 33, 58–66. [PubMed: 27295577]
3. Hewings DS; Rooney TP; Jennings LE; Hay DA; Schofield CJ; Brennan PE; Knapp S; Conway SJ Progress in the development and application of small molecule inhibitors of bromodomain-acetyl-lysine interactions. J Med Chem. 2012, 55, 9393–9413. [PubMed: 22924434]
4. Filippakopoulos P; Knapp S. Targeting bromodomains: epigenetic readers of lysine acetylation. Nat Rev Drug Discov. 2014, 13, 337–356. [PubMed: 24751816]
5. Smith SG; Zhou MM The Bromodomain: a new target in emerging epigenetic medicine. ACS Chem Biol. 2016, 11, 598–608. [PubMed: 26596782]
6. Vidler LR; Brown N; Knapp S; Hoelder S. Druggability analysis and structural classification of bromodomain acetyl-lysine binding sites. J Med Chem. 2012, 55, 7346–7359. [PubMed: 22788793]
7. Borah JC; Mujtaba S; Karakikes I; Zeng L; Muller M; Patel J; Moshkina N; Morohashi K; Zhang W; Gerona-Navarro G; Hajjar RJ; Zhou MM A small molecule binding to the coactivator CREB-binding protein blocks apoptosis in cardiomyocytes. Chem Biol. 2011, 18, 531–541. [PubMed: 21513889]
8. Cochran AG; Conery AR; Sims RJ 3rd. Bromodomains: a new target class for drug development. Nat Rev Drug Discov. 2019, 18, 609–628. [PubMed: 31273347]
9. Denny RA; Flick AC; Coe J; Langille J; Basak A; Liu S; Stock I; Sahasrabudhe P; Bonin P; Hay DA; Brennan PE; Pletcher M; Jones LH; Chekler ELP Structure-based design of highly selective inhibitors of the CREB binding protein Bromodomain. J Med Chem. 2017, 60, 5349–5363. [PubMed: 28375629]
10. Hay DA; Fedorov O; Martin S; Singleton DC; Tallant C; Wells C; Picaud S; Philpott M; Monteiro OP; Rogers CM; Conway SJ; Rooney TP; Tumber A; Yapp C; Filippakopoulos P; Bunnage ME; Müller S; Knapp S; Schofield CJ; Brennan PE Discovery and optimization of small-molecule ligands for the CBP/p300 bromodomains. J Am Chem Soc. 2014, 136, 9308–9319. [PubMed: 24946055]
11. Dancy BM; Cole PA Protein lysine acetylation by p300/CBP. Chem Rev. 2015, 115, 2419–52. [PubMed: 25594381]
12. Teufel DP; Freund SM; Bycroft M; Fersht AR Four domains of p300 each bind tightly to a sequence spanning both transactivation subdomains of p53. Proc Natl Acad Sci U S A. 2007, 104, 7009–7014. [PubMed: 17438265]
13. Plotnikov AN; Yang S; Zhou TJ; Rusinova E; Frasca A; Zhou MM Structural insights into acetylated-histone H4 recognition by the bromodomain-PHD finger module of human transcriptional coactivator CBP. Structure. 2014, 22, 353–360. [PubMed: 24361270]
14. Mujtaba S; He Y; Zeng L; Yan S; Plotnikova O; Sachchidanand; Sanchez R; Zeleznik-Le NJ; Ronai Z; Zhou MM Structural mechanism of the bromodomain of the coactivator CBP in p53 transcriptional activation. Mol Cell. 2004, 13, 251–263. [PubMed: 14759370]
15. Wimalasena VK; Wang T; Sigua LH; Durbin AD; Qi J. Using chemical epigenetics to target cancer. Mol Cell. 2020, 78, 1086–1095. [PubMed: 32407673]
16. Ghosh S; Taylor A; Chin M; Huang HR; Conery AR; Mertz JA; Salmeron A; Dakle PJ; Mele D; Cote A; Jayaram H; Setser JW; Poy F; Hatzivassiliou G; DeAlmeida-Nagata D; Sandy P; Hatton C; Romero FA; Chiang E; Reimer T; Crawford T; Pardo E; Watson VG; Tsui V; Cochran AG;

Zawadzke L; Harmange JC; Audia JE; Bryant BM; Cummings RT; Magnuson SR; Grogan JL; Bellon SF; Albrecht BK; Sims RJ 3rd; Lora JM Regulatory T cell modulation by CBP/EP300 bromodomain inhibition. J Biol Chem. 2016, 291, 13014–13027. [PubMed: 27056325]

17. Olzscha H; Fedorov O; Kessler BM; Knapp S; La Thangue NB CBP/p300 bromodomains regulate amyloid-like protein aggregation upon aberrant lysine acetylation. Cell Chem Biol. 2017, 24, 9–23. [PubMed: 27989401]
18. Giotopoulos G; Chan WI; Horton SJ; Ruau D; Gallipoli P; Fowler A; Crawley C; Papaemmanuil E; Campbell PJ; Göttgens B; Van Deursen JM; Cole PA; Huntly BJ The epigenetic regulators CBP and p300 facilitate leukemogenesis and represent therapeutic targets in acute myeloid leukemia. Oncogene. 2016, 35, 279–89. [PubMed: 25893291]
19. Brown PJ; Müller S. Open access chemical probes for epigenetic targets. Future Med Chem. 2015, 7, 1901–1917. [PubMed: 26397018]
20. Rooney TP; Filippakopoulos P; Fedorov O; Picaud S; Cortopassi WA; Hay DA; Martin S; Tumber A; Rogers CM; Philpott M; Wang M; Thompson AL; Heightman TD; Pryde DC; Cook A; Paton RS; Müller S; Knapp S; Brennan PE; Conway SJ A series of potent CREBBP bromodomain ligands reveals an induced-fit pocket stabilized by a cation-π interaction. Angew Chem Int Ed Engl. 2014, 53, 6126–6130. [PubMed: 24821300]
21. Chekler EL; Pellegrino JA; Lanz TA; Denny RA; Flick AC; Coe J; Langille J; Basak A; Liu S; Stock IA; Sahasrabudhe P; Bonin PD; Lee K; Pletcher MT; Jones LH Transcriptional profiling of a selective cREB Binding protein bromodomain inhibitor highlights therapeutic opportunities. Chem Biol. 2015, 22, 1588–1596. [PubMed: 26670081]
22. Popp TA; Tallant C; Rogers C; Fedorov O; Brennan PE; Müller S; Knapp S; Bracher F. Development of selective CBP/P300 benzoxazepine bromodomain inhibitors. J Med Chem. 2016, 59, 8889–8912. [PubMed: 27673482]
23. Taylor AM; Côté A; Hewitt MC; Pastor R; Leblanc Y; Nasveschuk CG; Romero FA; Crawford TD; Cantone N; Jayaram H; Setser J; Murray J; Beresini MH; de Leon Boenig G; Chen Z; Conery AR; Cummings RT; Dakin LA; Flynn EM; Huang OW; Kaufman S; Keller PJ; Kiefer JR; Lai T; Li Y; Liao J; Liu W; Lu H; Pardo E; Tsui V; Wang J; Wang Y; Xu Z; Yan F; Yu D; Zawadzke L; Zhu X; Zhu X; Sims RJ 3rd; Cochran AG; Bellon S; Audia JE; Magnuson S; Albrecht BK Fragment-based discovery of a selective and cell-active benzodiazepinone CBP/EP300 bromodomain Inhibitor (CPI-637). ACS Med Chem Lett. 2016, 7, 531–536. [PubMed: 27190605]
24. Crawford TD; Romero FA; Lai KW; Tsui V; Taylor AM; de Leon Boenig G; Noland CL; Murray J; Ly J; Choo EF; Hunsaker TL; Chan EW; Merchant M; Kharbanda S; Gascoigne KE; Kaufman S; Beresini MH; Liao J; Liu W; Chen KX; Chen Z; Conery AR; Côté A; Jayaram H; Jiang Y; Kiefer JR; Kleinheinz T; Li Y; Maher J; Pardo E; Poy F; Spillane KL; Wang F; Wang J; Wei X; Xu Z; Xu Z; Yen I; Zawadzke L; Zhu X; Bellon S; Cummings R; Cochran AG; Albrecht BK; Magnuson S. Discovery of a potent and selective in vivo probe (GNE-272) for the bromodomains of CBP/EP300. J Med Chem. 2016, 59, 10549–10563. [PubMed: 27682507]
25. Romero FA; Murray J; Lai KW; Tsui V; Albrecht BK; An L; Beresini MH; de Leon Boenig G; Bronner SM; Chan EW; Chen KX; Chen Z; Choo EF; Clagg K; Clark K; Crawford TD; Cyr P; de Almeida Nagata D; Gascoigne KE; Grogan JL; Hatzivassiliou G; Huang W; Hunsaker TL; Kaufman S; Koenig SG; Li R; Li Y; Liang X; Liao J; Liu W; Ly J; Maher J; Masui C; Merchant M; Ran Y; Taylor AM; Wai J; Wang F; Wei X; Yu D; Zhu BY; Zhu X; Magnuson S. GNE-781, a highly advanced potent and selective bromodomain inhibitor of cyclic adenosine monophosphate response element binding protein, binding protein (CBP). J Med Chem. 2017, 60, 9162–9183. [PubMed: 28892380]
26. McKeown MR; Shaw DL; Fu H; Liu S; Xu X; Marineau JJ; Huang Y; Zhang X; Buckley DL; Kadam A; Zhang Z; Blacklow SC; Qi J; Zhang W; Bradner JE Biased multicomponent reactions to develop novel bromodomain inhibitors. J Med Chem. 2014, 57, 9019–9127. [PubMed: 25314271]
27. Groebke K; Weber L; Mehlin F. Synthesis of imidazo[1,2-a] annulated pyridines, pyrazines and pyrimidines by a novel three-component condensation. Synlett. 1998, 1998, 661–663.

28. Blackburn C; Guan B; Fleming P; Shiosaki K; Tsai S. Parallel synthesis of 3-aminoimidazo[1,2-a]pyridines and pyrazines by a new three-component condensation. Tetrahedron Letters. 1998, 39, 3635–3638.
29. Bienaymé H; Bouzid K. A new heterocyclic multicomponent reaction for the combinatorial synthesis of fused 3-aminoimidazoles. Angew Chem Int Ed Engl. 1998, 37, 2234–2237. [PubMed: 29711433]
30. Suzuki A. Cross-coupling reactions of organoboranes: an easy way to construct C-C bonds (Nobel Lecture). Angew Chem Int Ed Engl. 2011, 50, 6722–6737. [PubMed: 21618370]
31. Roberts JM; Bradner JE A bead-based proximity assay for BRD4 ligand discovery. Curr Protoc Chem Biol. 2015, 7, 263–278. [PubMed: 26629616]
32. Seal J; Lamotte Y; Donche F; Bouillot A; Mirguet O; Gellibert F; Nicodeme E; Krysa G; Kirilovsky J; Beinke S; McCleary S; Rioja I; Bamborough P; Chung C-W; Gordon L; Lewis T; Walker AL; Cutler L; Lugo D; Wilson DM; Witherington J; Lee K; Prinjha RK Identification of a novel series of BET family bromodomain inhibitors: binding mode and profile of I-BET151 (GSK1210151A). Bioorg Med Chem Lett. 2012, 22, 2968–2972. [PubMed: 22437115]
33. Chaidos A; Caputo V; Gouvedenou K; Liu B; Marigo I; Chaudhry MS; Rotolo A; Tough DF; Smithers NN; Bassil AK; Chapman TD; Harker NR; Barbash O; Tummino P; Al-Mahdi N; Haynes AC; Cutler L; Le B; Rahemtulla A; Roberts I; Kleijnen M; Witherington JJ; Parr NJ; Prinjha RK; Karadimitris A. Potent antimyeloma activity of the novel bromodomain inhibitors I-BET151 and I-BET762. Blood. 2014, 123, 697–705. [PubMed: 24335499]
34. Filippakopoulos P; Picaud S; Mangos M; Keates T; Lambert J-P; Barsyte-Lovejoy D; Felletar I; Volkmer R; Müller S; Pawson T; Gingras A-C; Arrowsmith, Cheryl H; Knapp S. Histone recognition and large-scale structural analysis of the human bromodomain family. Cell. 2012, 149, 214–231. [PubMed: 22464331]
35. He ZX; Wei BF; Zhang X; Gong YP; Ma LY; Zhao W. Current development of CBP/p300 inhibitors in the last decade. Eur J Med Chem. 2020, 209, 112861.
36. Conery AR; Centore RC; Neiss A; Keller PJ; Joshi S; Spillane KL; Sandy P; Hatton C; Pardo E; Zawadzke L; Bommi-Reddy A; Gascoigne KE; Bryant BM; Mertz JA; Sims RJ Bromodomain inhibition of the transcriptional coactivators CBP/EP300 as a therapeutic strategy to target the IRF4 network in multiple myeloma. Elife. 2016, 5.
37. Galdeano C; Ciulli A. Selectivity on-target of bromodomain chemical probes by structure-guided medicinal chemistry and chemical biology. Future Med Chem. 2016, 8, 1655–1680. [PubMed: 27193077]
38. Lu Y; Zhang W. Microwave-assisted synthesis of a 3-aminoimidazo[1,2-a]-pyridine/pyrazine library by fluorous multicomponent reactions and subsequent cross-coupling reactions. QSAR Comb Sci. 2004, 23, 827–835. [PubMed: 18542716]
39. Gilson MK; Liu T; Baitaluk M; Nicola G; Hwang L; Chong J. BindingDB in 2015: A public database for medicinal chemistry, computational chemistry and systems pharmacology. Nucleic Acids Res. 2016, 44, D1045–1053. [PubMed: 26481362]
40. Kabsch W. Integration, scaling, space-group assignment and post-refinement. Acta Crystallogr D Biol Crystallogr. 2010, 66, 133–144. [PubMed: 20124693]
41. Afonine PV; Grosse-Kunstleve RW; Chen VB; Headd JJ; Moriarty NW; Richardson JS; Richardson DC; Urzhumtsev A; Zwart PH; Adams PD phenix.model_vs_data: a high-level tool for the calculation of crystallographic model and data statistics. J Appl Crystallogr. 2010, 43, 669–676. [PubMed: 20648263]
42. Emsley P; Lohkamp B; Scott WG; Cowtan K. Features and development of Coot. Acta Crystallogr D Biol Crystallogr. 2010, 66, 486–501. [PubMed: 20383002]

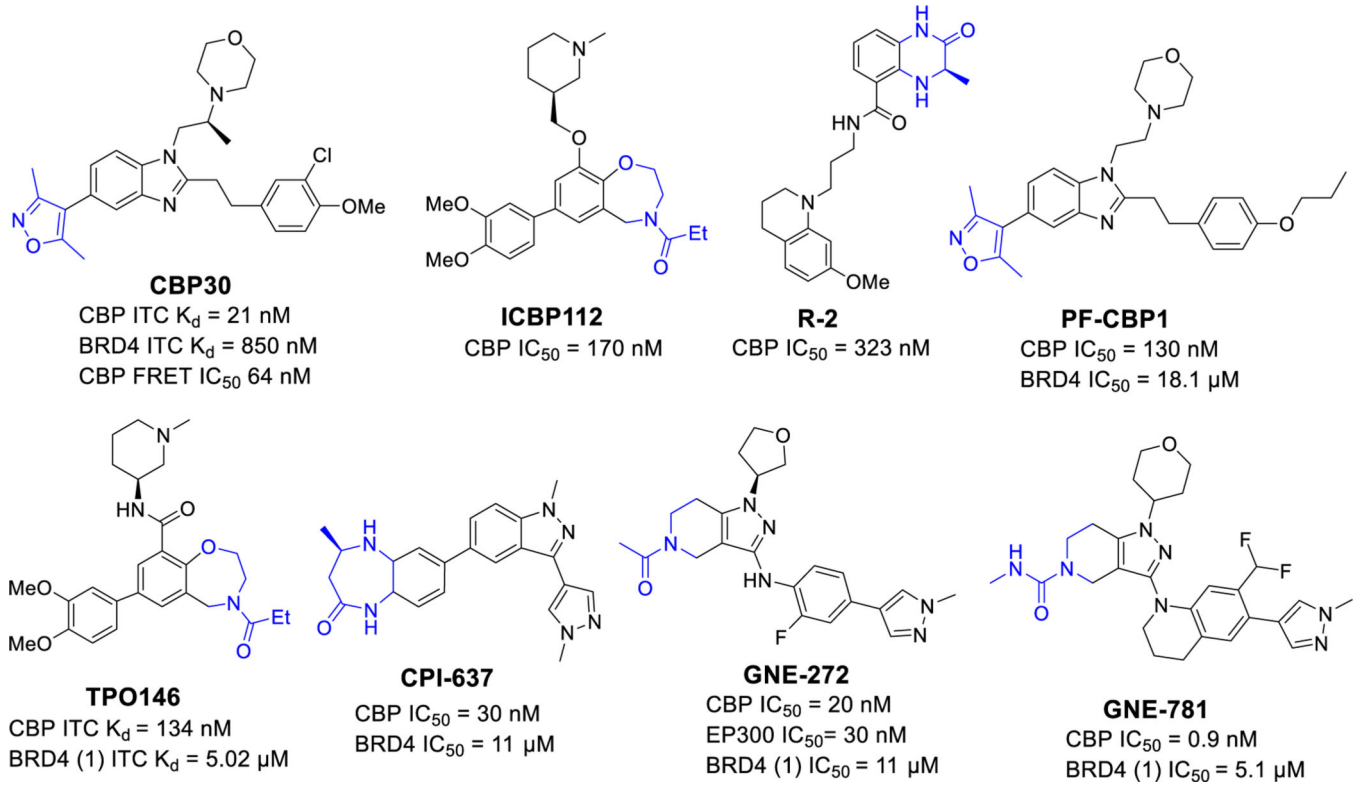

Figure 1.
Reported potent CBP inhibitors.

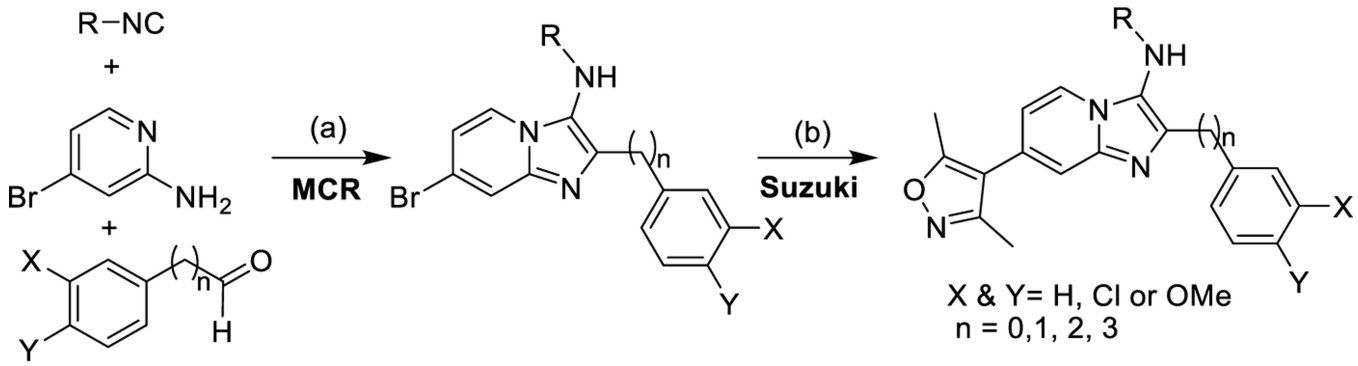

Reaction conditions: (a) $Sc(OTf)_3$, CH_2Cl_2/MeOH (3:1), μw,100 °C, 40 min 90-95%; (b) 3,5-dimethylisoxazole-4-boronic acid pinacol ester, $PdCl_2(dppf).CH_2Cl_2$, K_2CO_3, DME/H_2O (2:1), μw, 120 °C, 40 min, 89-93%.

Scheme 1.
Two-step synthesis of imidazo[1,2-*a*]pyridine-based CBP/P300 inhibitors.

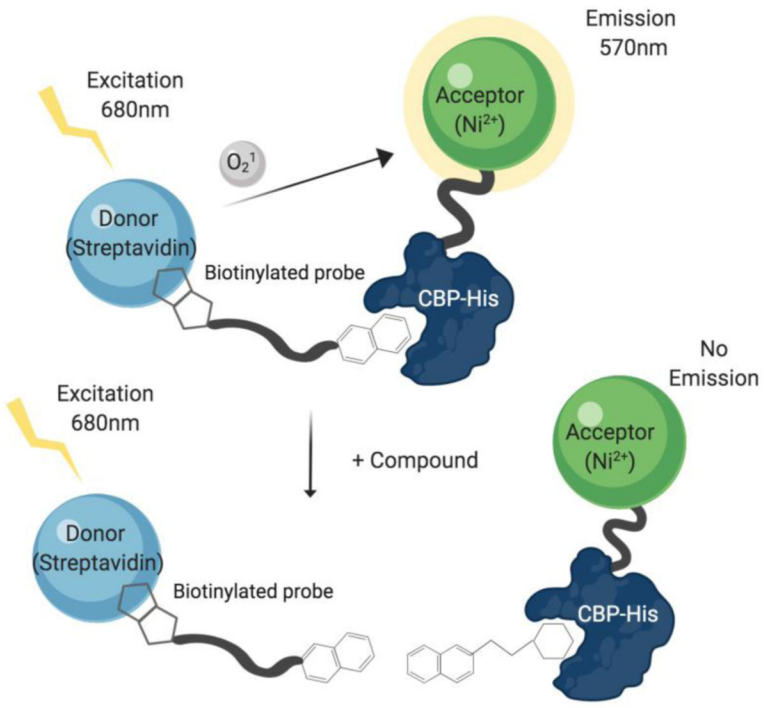

Figure 2.
Development of small molecule based CBP/P300 AlphaScreening assays.

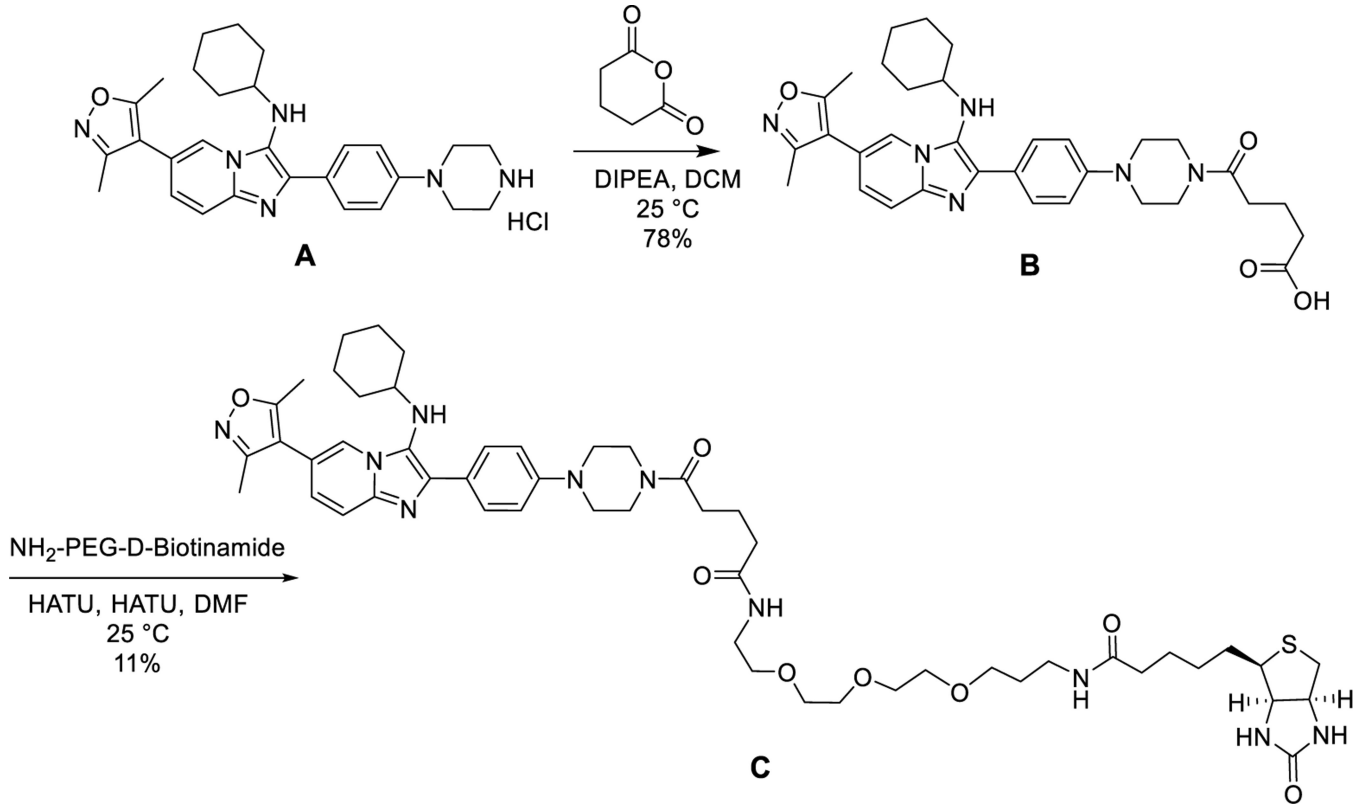

Scheme 2.

Synthesis of biotinylated-CBP/P300 bromodomain binder for AlphaScreening assay development.

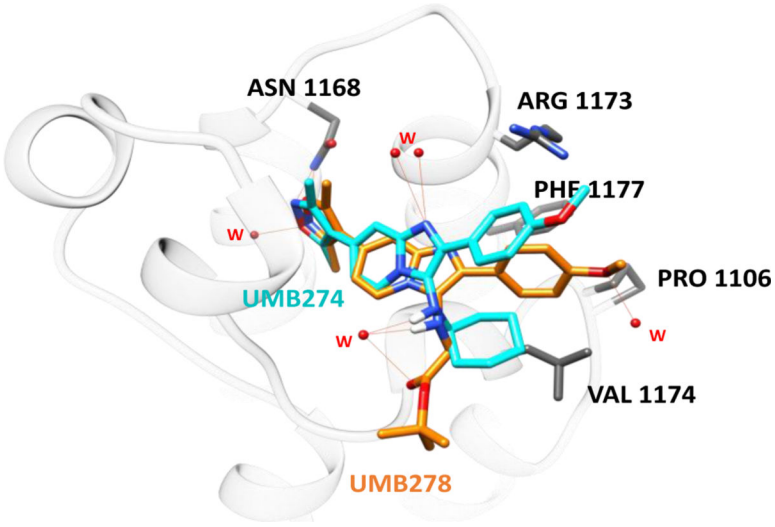

Figure 3.
Docked poses of compound **3** (cyan) and **4** (orange) in CBP (PDBs: 4NR7).

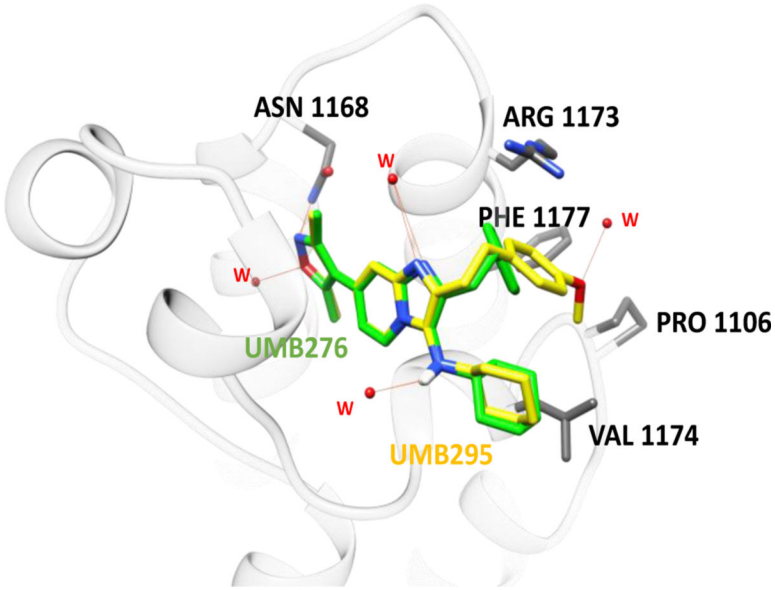

Figure 4.

Docked poses of compounds **7** (UMB276, green) and **16** (UMB295, yellow) in CBP. PDBs (4NR7 for CBP).

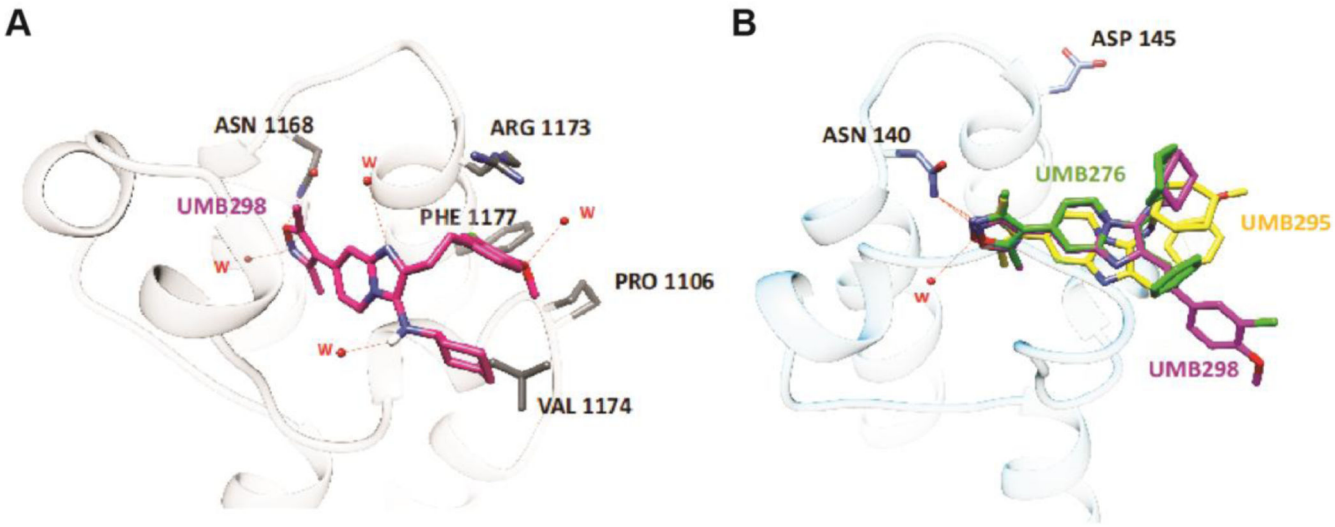

Figure 5. Docking pose of compound 23.

(A) Docked poses of compound **23** (UMB298) (magenta) in CBP. (B) Docked poses of compounds **7** (UMB276) (green), **16** (UMB295) (yellow) **23** (UMB298) (magenta) in BRD4. Water molecules are denoted by W and residues are denoted by their 3-letter amino acid code and their residues number in their respective PDBs (4NR7 for CBP and 5BT4 for BRD4). Hydrogen bonds between the molecule and surrounding residues and water are shown with red lines.

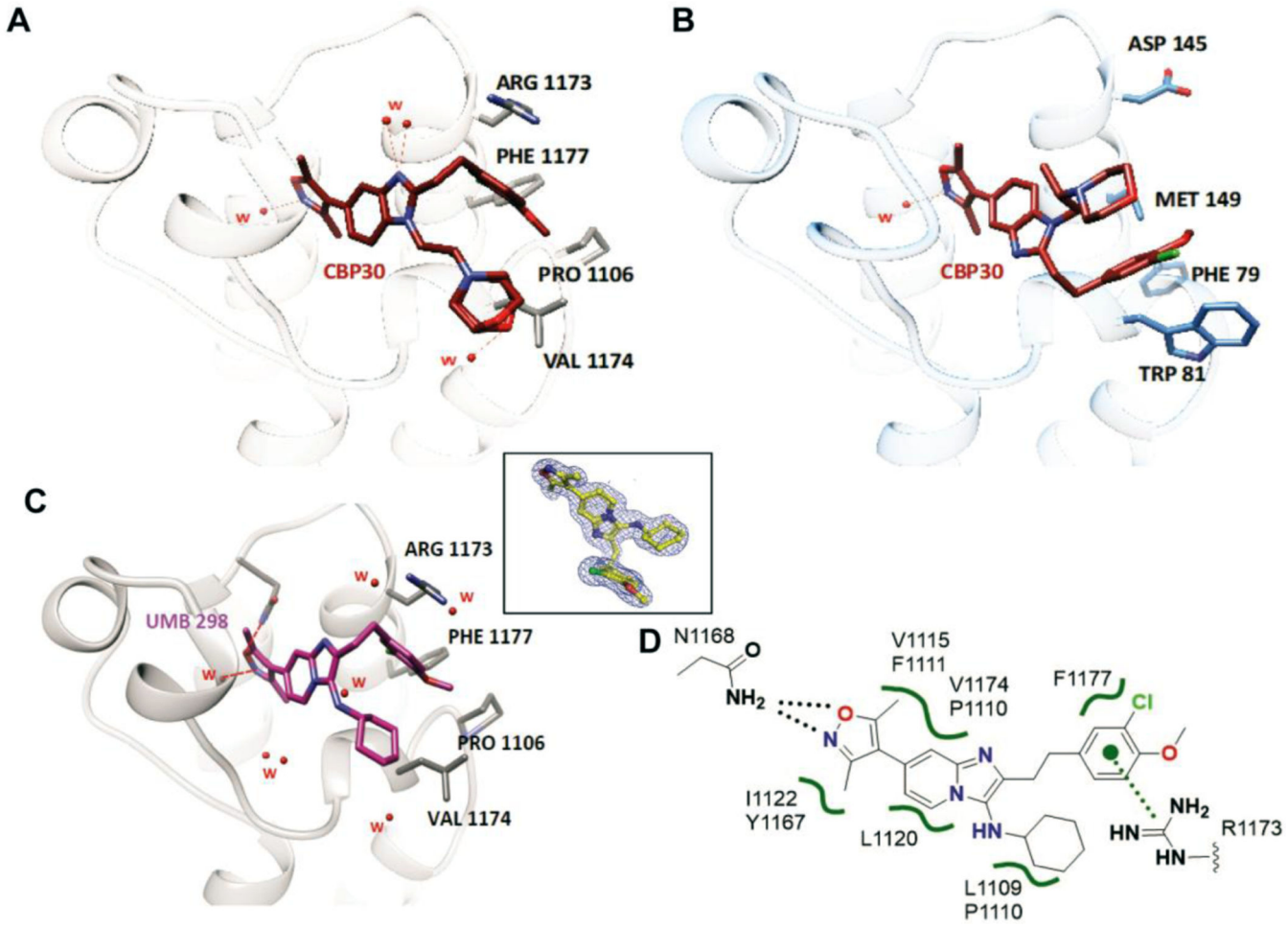

Figure 6.

Comparison of co-crystal structure of compound **23** with CBP30. (A) Crystal structures of CBP30 bound to CBP (left, PDB ID: 4NR7) and (B) BRD4 (right, PDB ID: 5BT4). Water molecules are denoted by W and residues are denoted by their 3-letter amino acid code. Hydrogen bonds between the molecule, surrounding residues and water are shown with red lines. (C) Compounds **23** (UMB298) (yellow) bound to the KAc site of CBP (grey) (PDB ID: 7KPY). H-bonds with Asn1168 (magenta) and water molecules (cyan) are indicated as black dotted lines. The inset shows the 2Fo-Fc electron density of the inhibitor. (D) Schematic presentation of H-bonding (black dotted lines) and hydrophobic van-der-Waals interactions (green wiggle lines) of UMB298 with KAc site residue. Arg1173 appears to establish cation-π interactions with the chloromethoxybenzene ring.

A

Protein	Compound	Tm (°C)	ΔTm (°C)
CBP	DMSO	46.7	0 ± 0.05
	Cpd 7	49.2	2.5 ± 0.03
	Cpd 16	51.5	4.8 ± 0.08
	Cpd 23	51.7	5.0 ± 0.07
	CBP30	55.2	8.5 ± 0.09
EP300	DMSO	42.1	0 ± 0.04
	Cpd 7	44.7	2.6 ± 0.05
	Cpd 16	46.8	4.8 ± 0.03
	Cpd 23	47.0	4.9 ± 0.03
	CBP30	50.6	8.6 ± 0.1
BRD4 (BD1)	DMSO	50.1	0 ± 0.04
	Cpd 7	51.0	0.9 ± 0.02
	Cpd 16	51.1	1.0 ± 0.07
	Cpd 23	50.1	0 ± 0.02
	CBP30	51.6	1.5 ± 0.1

B

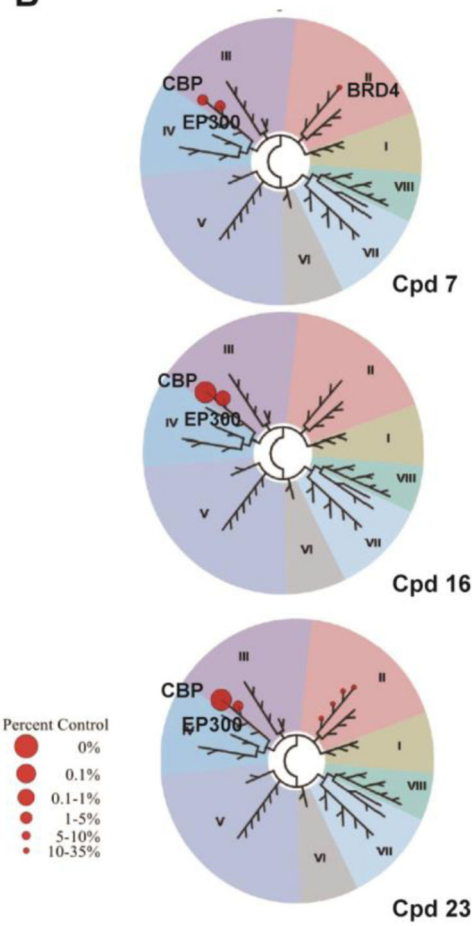

C

Targets	Cpd 16	Cpd 23	Cpd C
	Kd (nM)		
CREBBP	265 ± 35	315 ± 7	
EP300	285 ± 21	215 ± 35	13000 ± 2800
BRD4 (BD1)	9200 ± 400	>10000	

Figure 7.

Potency and selectivity profiling. (A). Tabulated temperature shift values of compound **7, 16, 23** and CBP30 with CBP (bromodomain), EP300 (bromodomain) and BRD4(BD1). (B). BROMOSCAN® data on compounds **7, 16, 23** against 34 bromodomains. (C). Kd value of compounds **16, 23** and biotinylated probe compound C toward CBP, EP300, and BRD4 (BD1) determined by BromoELECT®. All Kd is measured in duplicates followed the standard protocol developed by Eurofins.

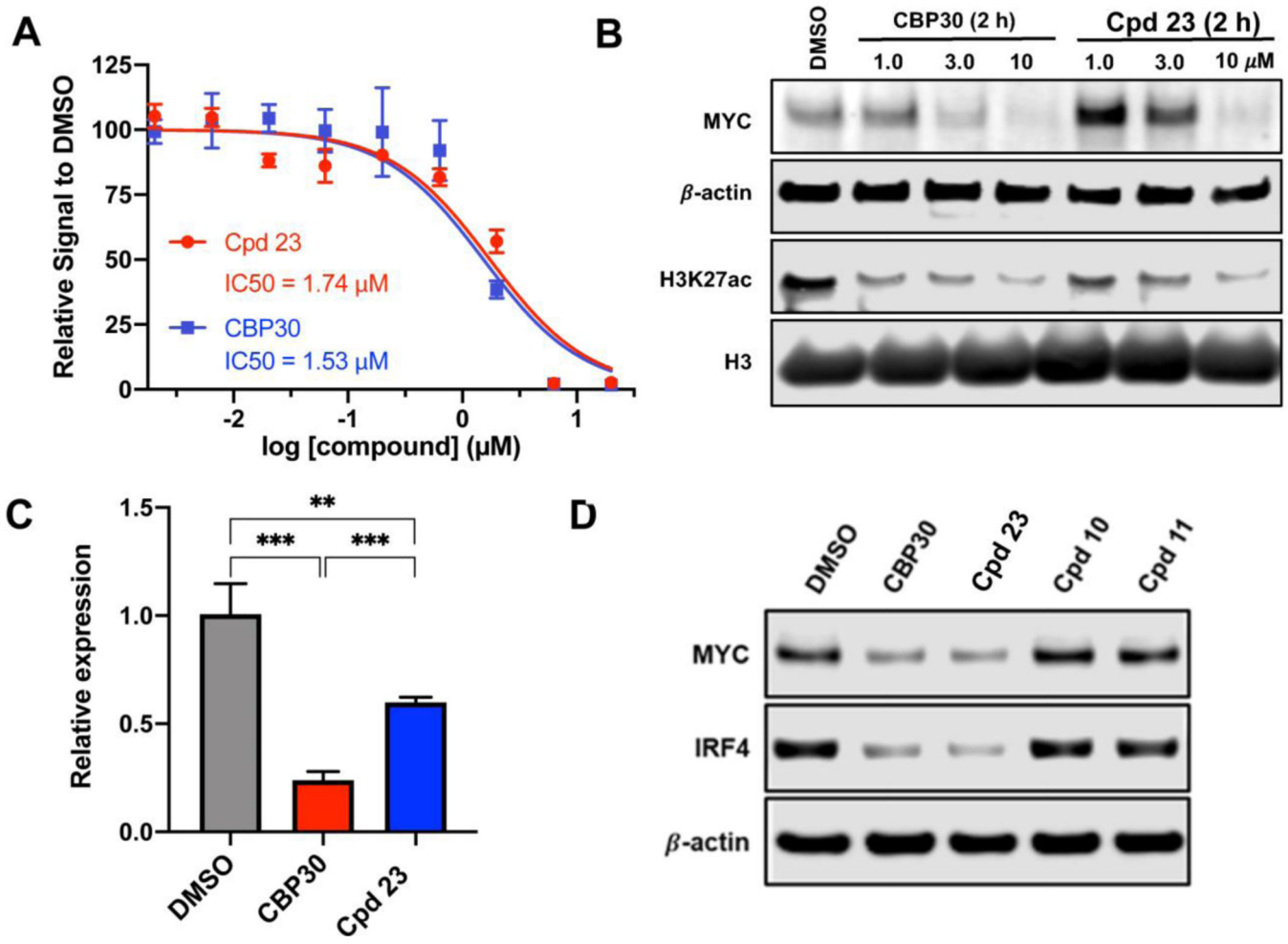

Figure 8.

Cellular activity of CBP/EP300 inhibitors in multiple myeloma cell lines. (A) Dose-proportional effect of CBP30 and compound **23** (UMB298) (5 day) on MOLM13 cellular viability as approximated by ATP-dependent luminescence (means ± SEM, n = 4). (B) Immunoblot of MYC, *β*-actin, H2K27ac and H3 following 2 h of incubation with DMSO or the indicated concentrations of CBP30 or compound **23** (UMB298) in MOLM13 cells. (C) Quantitative reverse transcription–polymerase chain reaction (RT-PCR) analysis of transcript levels of MYC after a 2-hour treatment of MOLM13 cells with DMSO, 3.0 μM CBP30, or 3.0 μM UMB298. Values represent three biologic replicates means ± SEM. *P = 0.01 to 0.05; **P = 0.001 to 0.01; ***P = 0.0001 to 0.001; ****P < 0.0001. (D) Immunoblot of MYC, IRF4 following 24 h incubation with DMSO or 2.5μM of CBP30, compound **23** (UMB298), compound **10** and compound **11** in MM.1S cells. *β*-actin is used as loading control.

Table 1.

Structure–Activity Relationship (SAR) on Imidazo[1,2-*a*]pyridine Scaffold

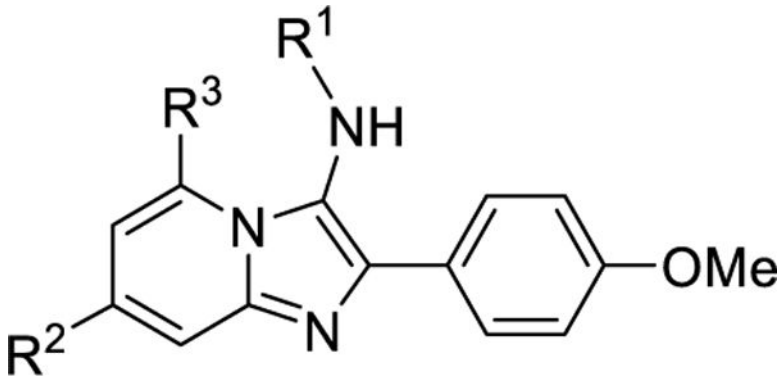

				IC$_{50}$ (μM)[a]		
Compound	**R^1**	**R^2**	**R^3**	**CBP**	**BRD4**	**Selectivity[b]**
1	adamantyl	Me	Me	16.09±0.76	>50	>3
2	adamantyl	3,5-dimethylisoxazolyl	H	2.21±0.43	>50	>23
3	cyclohexyl	3,5-dimethylisoxazolyl	H	14.19±0.81	>50	>4
4	***t*-butyl acetyl**	**3,5-dimethylisoxazolyl**	**H**	**1.17**±0.05	**2.95**±0.04	**3**
5	2,2,4-trimethylpentyl	Me	Me	16.33±0.53	>50	>3
CBP30				0.028±0.04	7.94±0.22	>100

[a] All IC$_{50}$ values are reported as means of values from at least four determinations. AlphaScreen assay with the isolated CBP (using biotinylated H3K56ac peptide)[34] or BRD4 bromodomain (with biotinylated JQ1).[31].

[b] Selectivity is defined by [BRD4(1) IC$_{50}$ (μM)/CBP IC$_{50}$ (μM)]

Table 2.

Structure–Activity Relationship on Compound 7 Analogs

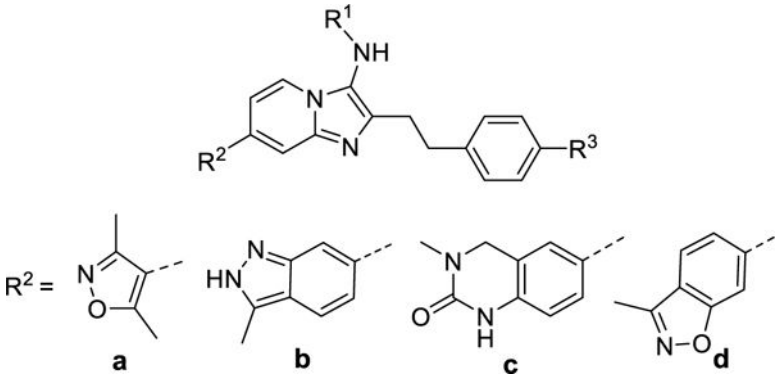

Compound	R^1	R^2	R^3	IC_{50} (μM)[a] CBP	IC_{50} (μM)[a] BRD4	Selectivity[b]
6	*t*-butyl acetyl	**a**	H	7.828	>50	>6
7 (UMB276)	cyclohexyl	**a**	H	0.718±0.042	7.43±1.18	10
8	adamantyl	**a**	H	0.507±0.045	3.38±0.63	7
9	cyclohexyl	**c**	H	8.12±0.96	7.55±0.56	1
10	cyclohexyl	**b**	H	8.02±0.06	0.51±0.01	0.06
11	cyclohexyl	**d**	H	>50	3.02±0.51	0.06
12	2,2,4-trimethylpentyl	**a**	H	1.88±0.03	2.77±0.08	1
13	*t*-butyl	**a**	H	0.95±0.02	5.63±0.31	6
14	adamantyl	**a**	OMe	0.923±0.012	7.11±0.31	8
15	4-ethylmorpholinyl	**a**	OMe	0.46±0.09	3.42±0.01	7
16	**cyclohexyl**	**a**	**OMe**	**0.159±0.021**	**6.59±0.05**	**41**
17	isopropyl	**a**	OMe	0.29±0.01	10.09±0.21	34
18	*t*-butyl	**a**	OMe	2.33±0.60	>50	>21
19	cyclohexyl	**a**	OEt	0.214±0.009	6.48±0.41	30
20	cyclohexyl	**a**	OPr	0.633±0.006	17.92±1.21	28
21	benzyl	**a**	OMe	1.92±0.12	8.46±0.55	4
22	4-chlorobenzyl	**a**	OMe	1.60±0.21	7.94±0.45	5
CBP30				0.077±0.011	10.1±0.55	>100

[a] All IC50 values are reported as means of values from at least two determinations. AlphaScreen assay with the isolated CBP (with compound C) or BRD4 (with biotinylated JQ1) bromodomain.

[b] Selectivity is defined by [BRD4(1) IC_{50} (μM)/CBP IC50 (μM)] for the consistency mentioned.

[c] The IC50 of compound 4 with CBP is measured using biotinylated peptide based AlphaScreen assay as Table 1.

Table 3.

Structure–Activity Relationship on compound 19 Analogs

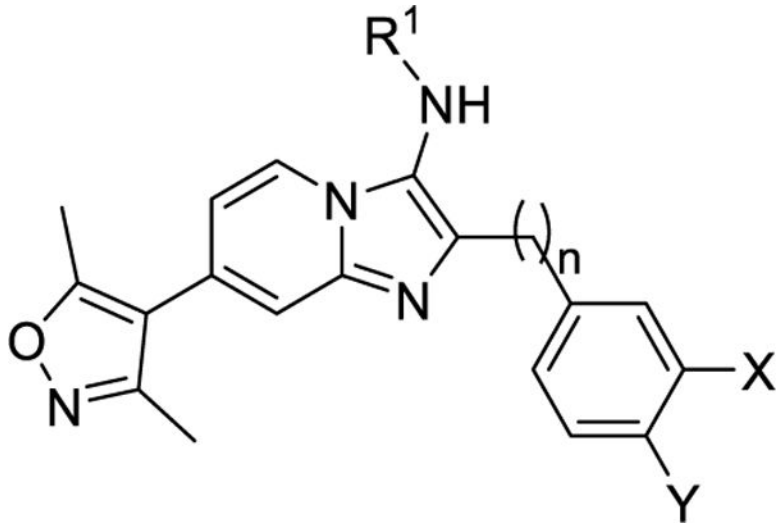

Compound	R^1	n	Y	X	IC_{50} (μM)[a] CBP	IC_{50} (μM)[a] BRD4	Selectivity[b]
16 (UMB295)	cyclohexyl	2	OMe	H	0.16±0.02	6.59±0.05	41
23 (UMB298)	**cyclohexyl**	**2**	**OMe**	**Cl**	**0.072±0.002**	**5.19±0.02**	**72**
24	cyclohexyl	1	OMe	H	6.07±0.04	11.22±1.01	2
25	cyclohexyl	3	OMe	H	4.95±0.41	12.33±1.11	3
26	2,2,4-trimethylpentyl	2	OMe	H	20.89±2.08	>50	>2
27	2,2,4-trimethylpentyl	2	OEt	H	38.49±7.12	>50	>1
28	2,2,4-trimethylpentyl	2	O*i*Pr	H	>50	>50	1
29	cyclohexyl	2	OEt	Cl	2.53±0.09	>50	20
30	cyclohexyl	3	OMe	Cl	8.96±0.91	24.53±2.33	3
31	2,2,4-trimethylpentyl	2	OEt	Cl	20.46±2.24	>50	>2
32	cyclohexyl	2	OMe	OMe	0.75±0.06	6.21±0.46	8
33	isopropyl	2	OMe	OMe	3.51±0.08	22.64±0.28	6
34	2,2,4-trimethylpentyl	3	OMe	H	>50	>50	1

[a] All IC50 values are reported as means of values from at least two determinations. AlphaScreen assay with the isolated CBP (with compound C) or BRD4 (with biotinylated JQ1) bromodomain.

[b] Selectivity is defined by [BRD4(1) IC50 (μM)/CBP IC50 (μM)] for the consistency mentioned.